

# A computational exploration of the McCoy–Tracy–Wu solutions of the third Painlevé equation<sup>1</sup>

Marco Fasondini<sup>2</sup>, Bengt Fornberg<sup>3</sup> and J.A.C. Weideman<sup>4</sup>

**Abstract.** The method recently developed by the authors for the computation of the multi-valued Painlevé transcendents on their Riemann surfaces (J. Comput. Phys. 344:36–50, 2017) is used to explore families of solutions to the third Painlevé equation that were identified by McCoy, Tracy and Wu (J. Math. Phys. 18:1058–1092, 1977) and which contain a pole-free sector. Limiting cases, in which the solutions are singular functions of the parameters, are also investigated and it is shown that a particular set of limiting solutions is expressible in terms of special functions. Solutions that are single-valued, logarithmically (infinitely) branched and algebraically branched, with any number of distinct sheets, are encountered. The algebraically branched solutions have multiple pole-free sectors on their Riemann surfaces that are accounted for by using asymptotic formulae and Bäcklund transformations.

**Key words.** Painlevé transcendents, P<sub>III</sub> equation, tronquée solutions, connection formulas, Bäcklund transformations, pole field solver

## 1 Introduction

The third Painlevé equation is the following second order nonlinear ODE defined in the complex plane,

$$P_{\text{III}} : \quad \frac{d^2 u}{dz^2} = \frac{1}{u} \left( \frac{du}{dz} \right)^2 - \frac{1}{z} \frac{du}{dz} + \frac{\alpha u^2 + \beta}{z} + \gamma u^3 + \frac{\delta}{u},$$

where  $\alpha, \beta, \gamma$  and  $\delta$  are arbitrary constants. It is one of six second order ODEs known as the Painlevé equations (denoted by P<sub>I</sub>–P<sub>VI</sub>) that were identified in the early 1900s [4, 14, 29, 30] as possessing the Painlevé property. This means that the solutions of the Painlevé equations, known as the Painlevé transcendents, have no movable branch point singularities. Movable poles, however, is a ubiquitous feature of the Painlevé transcendents and fixed branch points and fixed essential singularities [21, p. 128] are also possible. The Painlevé transcendents, as their name implies, generally cannot be expressed in terms of previously known functions [6]. They are notable not only for these and other analytical properties but also for their appearance in numerous and varied applications. For example, the P<sub>III</sub> equation appears in general relativity [31], the scattering of electromagnetic radiation [27], the Ising model [24] and the study of two-dimensional polymers [38] among others.

It follows from the Painlevé property that a Painlevé transcendent can have a branch point only at a fixed singularity of the Painlevé equation. Thus, we observe that in the finite complex plane, P<sub>III</sub> solutions can have a branch point only at  $z = 0$ . The third Painlevé transcendent is therefore generally multivalued, as are the fifth and sixth Painlevé transcendents, while P<sub>I</sub>, P<sub>II</sub> and P<sub>IV</sub> solutions are meromorphic and hence single-valued [15, Ch. 1].

---

<sup>1</sup>In this revised manuscript, changes to the material in the submitted manuscript are highlighted in yellow and new material is highlighted in green.

<sup>2</sup>University of the Free State, Department of Mathematics and Applied Mathematics, Bloemfontein 9300, South Africa (fasondinim@ufs.ac.za).

<sup>3</sup>University of Colorado, Department of Applied Mathematics, 526 UCB, Boulder, CO 80309, USA (fornberg@colorado.edu).

<sup>4</sup>Stellenbosch University, Department of Mathematical Sciences, Stellenbosch 7600, South Africa (weideman@sun.ac.za).

The pole field solver (PFS), introduced in [11], is the only numerical method yet presented that is capable of the efficient and accurate computation of the pole fields of the single-valued Painlevé transcendents on extended regions in the complex plane. Closed-form solutions to the Painlevé equations are known for special parameter values [8], but the PFS opened up the entire solution spaces of the  $P_I$ ,  $P_{II}$  and  $P_{IV}$  equations to computational exploration. Hence, the PFS enabled the study of unexplored  $P_I$ ,  $P_{II}$  and  $P_{IV}$  solutions, as reported in [11–13, 32–34]. In [9], we extended the PFS method to the computation of multivalued solutions of the  $P_{III}$ ,  $P_V$  and  $P_{VI}$  equations, thus making the solution spaces of these equations amenable to numerical exploration. This paper is the first application of this enhanced PFS method to the survey of a class of multivalued Painlevé transcendents.

In [25], McCoy, Tracy and Wu derived asymptotic formulae for  $P_{III}$  solutions with parameter values

$$\alpha = -\beta = 2\nu \quad \text{and} \quad \gamma = 1 = -\delta, \quad (1)$$

(if  $\gamma\delta \neq 0$ , one can set  $\gamma = 1 = -\delta$  without loss of generality in the  $P_{III}$  equation, see [15, p. 150]). We refer to the solutions that satisfy the asymptotic expansions of [25] as the MTW solutions. The derivation of the asymptotics was initiated by their earlier work (with E. Barouch) on the Ising model [3, 37], in which the third Painlevé equation arose in their analysis of the scaling limit of the spin-spin correlation functions. It is noted in [10] that, along with the paper by Ablowitz and Segur [1], the work of McCoy, Tracy, Wu and Barouch was responsible for the resurgence of interest in the Painlevé transcendents that occurred in the late 1970s. The reasons for this are (i) that [25] was the first rigorous study on connection formulae for the Painlevé transcendents, **which is made even more remarkable by its publication before the invention of the Riemann–Hilbert formalism for the Painlevé equations**, and (ii) [3, 37] were perhaps the first studies in which Painlevé equations featured in a physical application.

For fixed  $\nu$  the MTW solutions are a one-parameter family of  $P_{III}$  solutions that satisfy [25]

$$u(z; \nu, \lambda) \sim 1 - \lambda \Gamma\left(\nu + \frac{1}{2}\right) 2^{-2\nu} z^{-\nu-1/2} e^{-2z}, \quad z \rightarrow \infty, \quad -\frac{\pi}{2} < \arg z < \frac{\pi}{2}, \quad (2)$$

where  $\lambda$  is an arbitrary parameter. Hence, the MTW solutions are pole-free far out in the right half-plane, which make these solutions special since Painlevé transcendents typically have poles all over the complex plane. Solutions that contain a pole-free sector, such as the MTW solutions, have been known as tronquée solutions since 1913 [4], and have been identified and studied for the  $P_I$ – $P_V$  equations, see [2, 7, 17–20, 22, 35]. Furthermore, numerical evidence in [9] suggests that tronquée solutions of  $P_{VI}$  also exist. In particular, for  $P_{III}$  with  $\gamma = 1 = -\delta$ , Lin, Dai and Tibboel proved in [22] that for every  $\alpha$  and  $\beta$  there exist (i) a one-parameter family of tronquée solutions with  $u \sim 1$ ,  $z \rightarrow \infty$ ,  $-\pi/2 < \arg z < \pi/2$  and (ii) a unique tronquée solution with  $u \sim 1$ ,  $z \rightarrow \infty$ ,  $-\pi/2 < \arg z < 3\pi/2$ .<sup>5</sup> We refer to these tronquée solutions as the LDT solutions. The MTW solutions correspond to the one-parameter families of LDT solutions with  $\alpha = -\beta$ , as we shall show in section 2.1. Put differently, if we restrict  $\alpha$ ,  $\beta$  and the arbitrary parameter of the tronquée family ( $\lambda$ , in the case of the MTW solutions) to real values, as we shall do henceforth, then the MTW solutions correspond to the plane  $(\alpha, \beta, \lambda) = (2\nu, -2\nu, \lambda)$ ,  $\nu, \lambda \in \mathbb{R}$  in the parameter space of the LDT solutions. The MTW solutions on the line  $\lambda = 0$  in the parameter space correspond to the rational solution  $u = 1$ , see (2). According to the aforementioned results of Lin, Dai and Tibboel, this is the unique tronquée solution with a pole-free sector of angular width  $2\pi$  for the cases  $\alpha = -\beta$ .

The large- $z$  asymptotics of the LDT solutions are given in [22]. However, as far as we are aware, the MTW solutions are the only subset of the LDT solutions for which the connection

---

<sup>5</sup>Lin, Dai and Tibboel also proved the existence of other tronquée solutions. However, these solutions can be obtained by scaling and rotating the tronquée solutions with  $u \sim 1$ ,  $z \rightarrow \infty$  for  $-\pi/2 < \arg z < \pi/2$  or  $-\pi/2 < \arg z < 3\pi/2$ , i.e., by applying the transformation  $T_0$  defined and discussed in section 6.2.

formulae relating the large- $z$  and small- $z$  behaviors are known. As we shall find in section 6.2, the small- $z$  asymptotic formulae are crucial to an understanding of the symmetries and asymmetries that the MTW solutions exhibit between the different sheets of its Riemann surfaces. It is for these reasons that we singled out the MTW tronquée solutions for a first computational exploration.

The remainder of this work is structured as follows. We first present the large- $z$  and small- $z$  asymptotics of the MTW solutions. Recalling that the gamma function has simple poles at the non-positive integers, (2) implies that the cases  $\nu = -\frac{1}{2} - n$ , with  $n$  a nonnegative integer, require special attention. Hence, we divide the parameter space of the MTW solutions into the cases  $\nu > -\frac{1}{2}$ ,  $\nu < -\frac{1}{2}$  and the limiting cases  $\nu = -\frac{1}{2} - n$ . With the help of our numerical method, we first explore the MTW solutions for these cases on a single sheet,  $-\pi/2 < \arg z \leq \pi/2$ , and then on multiple sheets ( $|\arg z| > \pi/2$ ). Numerical results are presented in the form of modulus plots that show poles, zeros and branch cuts in the complex plane, which are complemented in some cases by plots of the phase of the solution.

## 2 The asymptotics of the MTW solutions

### 2.1 The large- $z$ asymptotics

The large- $z$  asymptotics of the LDT solutions discussed above is [22, eqs. (1.7) and (2.14)]

$$u \sim 1 + \sum_{j=1}^{\infty} \frac{a_j}{z^j} - kz^d e^{-2z}, \quad z \rightarrow \infty, \quad -\frac{\pi}{2} < \arg z < \frac{\pi}{2},$$

where  $k$  is an arbitrary parameter. The PFS used for generating the solution diagrams presented in this paper require starting values,  $u$  and  $u'$ . These will be obtained from expansions such as the one above using the optimal truncation rule. To improve the accuracy of this particular expansion we use the ansatz

$$u \sim 1 + \sum_{j=1}^{\infty} \frac{a_j}{z^j} - kz^d e^{-2z} \left( 1 + \sum_{j=1}^{\infty} \frac{c_j}{z^j} \right), \quad z \rightarrow \infty, \quad -\frac{\pi}{2} < \arg z < \frac{\pi}{2}, \quad (3)$$

to obtain higher order terms. Substituting (3) into  $P_{\text{III}}$  with  $\gamma = 1 = -\delta$  and matching terms we find that

$$d = \frac{1}{4}(\beta - \alpha) - \frac{1}{2}, \quad (4)$$

and that the  $a_j$  and  $c_j$  are polynomial functions of  $\alpha$  and  $\beta$ . One can show, using the recursive formulas for  $a_j$  in [22], that for the MTW parameters (1),  $a_j = 0$ ,  $j \geq 1$ . Thus, if we set  $k = \lambda \Gamma(\nu + \frac{1}{2}) 2^{-2\nu}$  then, with MTW parameters  $\alpha = -\beta = 2\nu$ , (4) and (3) become (cf. (2)),

$$u(z; \nu, \lambda) \sim 1 - \lambda \Gamma(\nu + \frac{1}{2}) 2^{-2\nu} z^{-\nu-1/2} e^{-2z} \left( 1 + \sum_{j=1}^{\infty} \frac{c_j}{z^j} \right), \quad z \rightarrow \infty, \quad -\frac{\pi}{2} < \arg z < \frac{\pi}{2}. \quad (5)$$

If we multiply the  $P_{\text{III}}$  equation with MTW parameters by  $u$  and expand  $u$  as in (3) with  $a_j = 0$ , then we find that, for  $z \rightarrow \infty$ ,  $-\frac{\pi}{2} < \arg z < \frac{\pi}{2}$ ,

$$kz^{-\nu-1/2} e^{-2z} \sum_{j=0}^{\infty} \left[ -4(j+1)c_{j+1} - \frac{1}{4}(2\nu+2j+1)^2 c_j \right] z^{-j-2} + \mathcal{O}(e^{-4z}) \sim 0,$$

and thus the coefficients are given by

$$c_{j+1} = -\frac{(2\nu + 2j + 1)^2}{16(j+1)}c_j, \quad j \geq 0, \quad c_0 = 1. \quad (6)$$

It suffices to consider only  $\lambda > 0$  since it is shown in [25] that

$$u(z; \nu, -\lambda) = \frac{1}{u(z; \nu, \lambda)}. \quad (7)$$

The formula (5) is not valid for the values  $\nu = -\frac{1}{2} - n$ ,  $n \geq 0$ . However, there are solutions with  $\nu = -\frac{1}{2} - n$  that are related to the MTW solutions, which we discuss in section 5.

## 2.2 The small- $z$ asymptotics

### 2.2.1 $0 < \lambda < 1/\pi$ or $0 < \sigma < 1$

The  $P_{\text{III}}$  equation with MTW parameters admits the formal small- $z$  expansion

$$u(z/2) \sim Bz^\sigma \left\{ 1 + \sum_{j=1}^{\infty} \sum_{k=1}^{j+1} b_{j,k} z^{j-\sigma(j+2-2k)} \right\}, \quad z \rightarrow 0, \quad -1 < \text{Re } \sigma < 1, \quad (8)$$

where  $B$  is arbitrary and the  $b_{j,k}$  are **unique** functions of  $\sigma$ ,  $\nu$  and  $B$  [25]. It transpires that  $b_{j,1} = 0$ ,  $j \geq 3$  [25], which implies that there are no terms of the form  $z^{n-n\sigma}$  for  $n \geq 3$ , and thus (8) becomes

$$u(z/2) = Bz^\sigma \{ 1 + b_{1,1}z^{1-\sigma} + b_{1,2}z^{1+\sigma} + b_{2,1}z^{2-2\sigma} + \mathcal{O}(z^2) \}, \quad -1 < \text{Re } \sigma < 1, \quad (9)$$

where [25]

$$Bb_{1,1} = -\frac{\nu}{(1-\sigma)^2}, \quad Bb_{1,2} = \frac{B^2\nu}{(\sigma+1)^2}, \quad \text{and} \quad Bb_{2,1} = \frac{1}{B} \left[ \frac{4\nu^2 - (\sigma-1)^2}{16(\sigma-1)^4} \right]. \quad (10)$$

If the large- $z$  behavior of the solution is given by (2), then  $\sigma$  and  $B$  are no longer arbitrary but they become functions of  $\lambda$  and  $\nu$ . Specifically, as demonstrated in [25], the connection formulae relating the large- $z$  behavior, (2), and the small- $z$  behavior, (9), are given by

$$\sigma = \sigma(\lambda) = \frac{2}{\pi} \arcsin(\pi\lambda), \quad (11)$$

and

$$B = B(\sigma, \nu) = 2^{-3\sigma} \frac{\Gamma^2(\frac{1}{2}(1-\sigma)) \Gamma(\frac{1}{2}(1+\sigma) + \nu)}{\Gamma^2(\frac{1}{2}(1+\sigma)) \Gamma(\frac{1}{2}(1-\sigma) + \nu)}. \quad (12)$$

Since we let  $\lambda > 0$ , we only consider (9)–(12) for  $0 < \sigma < 1$ , or  $0 < \lambda < 1/\pi$ . Henceforth we use the notations  $u(z; \nu, \lambda)$  and  $u(z; \nu, \sigma)$  interchangeably to denote the MTW solutions.

Note from (12) that  $B(\sigma, \nu)$  vanishes when  $\Gamma(\frac{1}{2}(1-\sigma) + \nu)$  is singular, i.e.,

$$B(\sigma, \nu) \rightarrow 0, \quad \sigma \rightarrow \sigma_c = 2\nu + 2n + 1, \quad -n - \frac{1}{2} < \nu < -n, \quad n \geq 0, \quad (13)$$

where the inequality follows from the condition  $0 < \sigma_c < 1$ . Likewise,  $B(\sigma, \nu)$  becomes unbounded if a pole of  $\Gamma(\frac{1}{2}(1+\sigma) + \nu)$  is approached:

$$|B(\sigma, \nu)| \rightarrow \infty, \quad \sigma \rightarrow \sigma_c = -2\nu - 2n - 1, \quad -n - 1 < \nu < -n - \frac{1}{2}, \quad n \geq 0. \quad (14)$$

The behavior of the coefficients  $B(\sigma, \nu)b_{1,1}$  and  $B(\sigma, \nu)b_{1,2}$  in (10) in the limits (13) and (14) is clear. The coefficient  $B(\sigma, \nu)b_{2,1}$ , however, is bounded in the limit (13) if  $n = 0$  but unbounded if  $n > 0$ :

$$\lim_{\sigma \rightarrow 2\nu+1} B(\sigma, \nu)b_{2,1} = \frac{2^{6\nu}\Gamma^2(\nu)}{8\nu^2\Gamma^2(-\nu)\Gamma(2\nu)}, \quad -\frac{1}{2} < \nu < 0, \quad (15)$$

$$B(\sigma, \nu)b_{2,1} \sim -\frac{n(n+2\nu)}{64(n+\nu)^4} \frac{1}{B(\sigma, \nu)}, \quad B(\sigma, \nu) \rightarrow 0, \quad (16)$$

where  $\sigma \rightarrow 2\nu + 2n + 1$ ,  $-n - \frac{1}{2} < \nu < -n$  and  $n \geq 1$  in (16). We shall consider the MTW solutions in the complex plane in the limits (13) and (14) in section 4.2.

### 2.2.2 $\lambda = 1/\pi$ or $\sigma = 1$

The following small- $z$  asymptotic formulae for  $\lambda \geq 1/\pi$  are valid on the positive real axis,  $\mathbb{R}^+$ , which we indicate by using the variable  $x$ . It is shown in [25] that in the limit  $\lambda \rightarrow 1/\pi$ , or  $\sigma \rightarrow 1$ , (9)–(12) become

$$u(x/2; \nu, \pi^{-1}) \sim \frac{1}{2}x \left\{ \nu \ln^2 x - C(\nu) \ln x + \frac{1}{4\nu} [C^2(\nu) - 1] \right\}, \quad x \rightarrow 0^+, \quad (17)$$

where

$$C(\nu) = 1 + 2\nu[3 \ln 2 + 2\psi(1) - \psi(\nu + 1)]. \quad (18)$$

Here  $\psi$  denotes the digamma function ( $\psi = \Gamma'/\Gamma$ ) and  $\lim_{\nu \rightarrow 0} 1/(4\nu)[C^2(\nu) - 1] = 3 \ln 2 + \psi(1)$ . The cases

$$\nu = -n, \quad n \geq 1, \quad (19)$$

for which the constant  $C(\nu)$  becomes unbounded will be discussed in section 4.2. The cases (19) can be considered as special cases of the large- $B$  limit (14) with  $\nu \rightarrow -n - 1$  and thus  $\sigma_c \rightarrow 1$ .

### 2.2.3 $\lambda > 1/\pi$ or $\sigma = 1 + 2i\mu$ , $\mu > 0$

Small- $x$  asymptotic formulae for  $\lambda > 1/\pi$  were derived in [25] only for  $\nu = 0$ . Here we also consider the case  $\nu \neq 0$ ,  $\nu \in \mathbb{R}$ . For  $\lambda > 1/\pi$ , we let

$$\lambda = \cosh(\pi\mu)/\pi, \quad \mu > 0, \quad \implies \quad \sigma = 1 + 2i\mu. \quad (20)$$

Using the properties  $\Gamma(1+z) = z\Gamma(z)$  and  $\Gamma(\bar{z}) = \overline{\Gamma(z)}$ , (12) becomes

$$\begin{aligned} B(1 + 2i\mu, \nu) &= 2^{-3-6i\mu} \frac{\Gamma^2(-i\mu)\Gamma(1+\nu+i\mu)}{\Gamma^2(1+i\mu)\Gamma(\nu-i\mu)} \\ &= -\frac{(\nu+i\mu)}{8\mu^2} \exp \{2i [\arg \Gamma(\nu+i\mu) - 2 \arg \Gamma(i\mu) - \mu \log 8]\} \end{aligned} \quad (21)$$

and for  $x \rightarrow 0^+$  (9) and (10) simplify to

$$\begin{aligned} u(x/2; \nu, \cosh(\pi\mu)/\pi) &= B(1 + 2i\mu, \nu)x [b_{1,1} + x^{2i\mu} + b_{2,1}x^{-2i\mu}] + \mathcal{O}(x^3), \\ &= x \left[ \frac{\nu}{4\mu^2} + B(1 + 2i\mu, \nu)x^{2i\mu} + \overline{B(1 + 2i\mu, \nu)}x^{-2i\mu} \right] + \mathcal{O}(x^3), \\ &= \frac{x}{4\mu} \left\{ \frac{\nu}{\mu} (1 - \cos [\phi(x, \nu, \mu)]) + \sin [\phi(x, \nu, \mu)] \right\} + \mathcal{O}(x^3), \end{aligned} \quad (22)$$

where

$$\phi(x, \nu, \mu) = 2\mu \ln(x/8) - 4 \arg [\Gamma(i\mu)] + 2 \arg [\Gamma(\nu + i\mu)]. \quad (23)$$

### 2.3 An example of an MTW solution

The bottom-left frame of Figure 1 depicts the modulus of an MTW solution with parameters  $\nu = \frac{1}{2}$  and  $\mu = 2$  (see (20)) on the annulus  $10^{-10} \leq |z| \leq 15$ ,  $-\pi < \arg z \leq \pi$ . We shall find it instructive to depict some solutions in the  $\zeta$ -plane, which is related to the  $z$ -plane according to  $z = e^{\zeta/2}$ . The  $\zeta$ -plane region corresponding to the annulus in the  $z$ -plane is the rectangle  $-2\pi < \text{Im } \zeta \leq 2\pi$ ,  $2 \log(10^{-10}) \leq \text{Re } \zeta \leq 2 \log(15)$ , see the top frame of Figure 1. Since the branch point at  $z = 0$  is mapped out of the finite  $\zeta$ -plane, the solution is meromorphic in the  $\zeta$ -plane [16]. As noted in [9], this makes it convenient to compute  $P_{\text{III}}$  solutions in the  $\zeta$ -plane, which is the approach we used to compute the MTW solutions. Henceforth we refer to the solution on the region  $-\pi < \arg z - 2\pi s \leq \pi$ , or  $-2\pi < \text{Im } \zeta - 4\pi s \leq 2\pi$ , as the solution on the  $s$ -th sheet of the Riemann surface. We indicate the presence of a branch cut in the  $z$ -plane with a dashed line on the negative real axis ( $\mathbb{R}^-$ ). For the MTW parameter values (1), the poles of  $P_{\text{III}}$  solutions are of first order with residue  $+1$  or  $-1$  in the  $z$ -plane, indicated by red and yellow circles, respectively, see Table 1. The zeros of the MTW solutions are simple and are indicated by squares, likewise described in Table 1. Conspicuous in the bottom-left frame is the pole-free sector contained in the right half-plane, in accordance with the large- $z$  formula (5). The poles are arranged as spirals in the  $z$ -plane which, as noted in [9], appears to be a common feature of the multivalued (but not the meromorphic) Painlevé transcendents. The modulus of the solution has an up-down symmetry in the  $z$  and  $\zeta$  planes since the solution in the upper and lower half planes are conjugate. This is a consequence of the fact that for real parameter values, the MTW solutions are real on  $\arg z = 0$  (which corresponds to the real  $\zeta$ -axis), as indicated by the asymptotic formulae above.

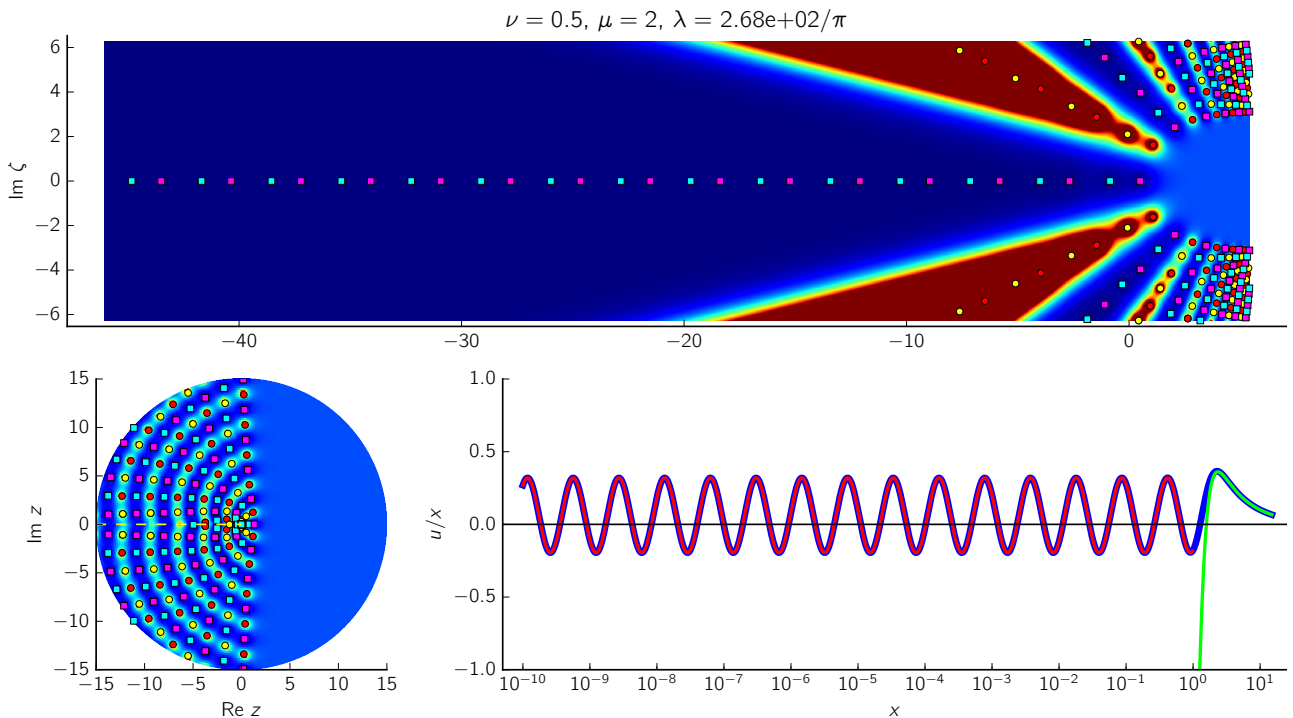


Figure 1: An MTW solution with  $\nu > -\frac{1}{2}$  for the case  $\lambda > 1/\pi$  on the annulus  $10^{-10} \leq |z| \leq 15$  (bottom-left frame), its corresponding region in the  $\zeta$ -plane (top frame,  $z = e^{\zeta/2}$ ) and on the positive real axis of the  $z$ -plane (bottom-right frame). In the latter frame the small- $x$  and large- $x$  asymptotic approximations, (22) (red) and (5) (green), respectively, are divided by  $x$  and superimposed on the computed solution (blue), which is also divided by  $x$ .

Table 1: The markers used in the diagrams to indicate poles and zeros of the MTW solutions in the  $z$  and  $\zeta$  planes ( $z = e^{\zeta/2}$ ). In a neighborhood of a pole or zero at  $z_0$  one has  $u \approx c_k(z - z_0)^k$  with  $k < 0$  or  $k > 0$ , respectively. Making this substitution in  $P_{\text{III}}$  and taking the limit  $z \rightarrow z_0$  readily yields the order  $k$  of the pole or zero as well as the leading order coefficient  $c_k$ . We assume that  $z_0 \neq 0$  (poles and zeros at the origin will be discussed in section 4.2). A simple pole (or a simple zero) at  $z_0$  with residue  $\pm 1$  (or  $c_1 = u'(z_0) = \pm 1$ ) corresponds to a simple pole (or a simple zero) at  $\zeta_0 = 2 \log z_0$  in the  $\zeta$ -plane with residue  $\pm 1/\frac{dz}{d\zeta} = \pm 2e^{-\zeta_0/2}$  (or  $c_1 = \pm \frac{dz}{d\zeta} = \pm \frac{1}{2}e^{\zeta_0/2}$ ).

	Poles		Zeros	
$z$ -plane	$c_{-1} = +1$	●	$c_1 = +1$	■
	$c_{-1} = -1$	●	$c_1 = -1$	■
$\zeta$ -plane	$c_{-1} = +2e^{-\zeta_0/2}$	●	$c_1 = +\frac{1}{2}e^{\zeta_0/2}$	■
	$c_{-1} = -2e^{-\zeta_0/2}$	●	$c_1 = -\frac{1}{2}e^{\zeta_0/2}$	■

The bottom-right frame of Figure 1 shows the solution on  $\arg z = 0$  with the **large- $x$**  (5) and **small- $x$**  (22) **asymptotic formulae; note how these formulae match the computed solution.** As expected from (22), the solution is oscillatory with an infinite number of zeros accumulating on  $\arg z = 0$  as  $z \rightarrow 0$  for  $\lambda > 1/\pi$ . If  $\lambda < -1/\pi$ , infinitely many poles accumulate on  $\mathbb{R}^+$ , see (7), in which case the limit point  $z = 0$  is a non-isolated singularity. For fixed  $\nu$ , the poles or zeros become more closely spaced on the real  $\zeta$ -axis as  $\mu$  increases, see (22) and (23). For fixed  $\nu$  and  $\mu$ , the spacing of the poles or zeros on the real  $\zeta$ -axis is uniform, see Figure 1 and (23) with  $x = e^{\zeta/2}$ , which implies that in the  $z$ -plane the spacing is proportional to  $z$  **and thus decreases exponentially** as  $z \rightarrow 0$  on  $\arg z = 0$ .

### 3 MTW solutions with $\nu > -\frac{1}{2}$ on the 0th sheet

#### 3.1 Fixed $\nu$ , varying $\lambda$

For MTW solutions with a fixed value of  $\nu$ , where  $\nu > -\frac{1}{2}$ , the pole field dynamics on the 0th sheet can be divided into three stages:  $0 < \lambda \leq \lambda_c$  (recall that  $\lambda = 0$  corresponds to the solution  $u = 1$ ),  $\lambda_c < \lambda \leq 1/\pi$  and  $\lambda > 1/\pi$ . Figure 2 depicts pole fields in these stages. In the first stage, as  $\lambda$  is increased from zero, a pole field moves horizontally to the right from the left half-plane (leftmost frame). In the second stage, the moment  $\lambda$  exceeds  $\lambda_c$  (our computations indicate that  $\lambda_c \approx 0.1/\pi$ ) then, in addition to the horizontal rightwards movement of the pole field for increasing  $\lambda$ , there is also a slight vertical movement upwards (in the upper half-plane) and downwards (in the lower half-plane) as poles from the neighboring sheets (sheets +1 and -1) move through the branch cut (middle frame). In the third stage, as  $\lambda$  is increased beyond  $1/\pi$ , the branch point  $z = 0$  acts as a ‘zeros source’ along  $\mathbb{R}^+$  according to (22) and the movement of poles into the right half-plane along arcs that emerge through the branch cut is continued (rightmost frame). If we compare the middle frame of Figure 2 (for which  $\mu = 0$ ), the bottom left frame of Figure 1 ( $\mu = 2$ ) and the rightmost frame of Figure 2 ( $\mu = 5$ ), we find that in the upper half-plane there are poles on five, six and eight arcs, respectively. In these frames the numbers of poles in the annulus  $10^{-10} \leq |z| \leq 5$  are, respectively, 8, 37 and 172.

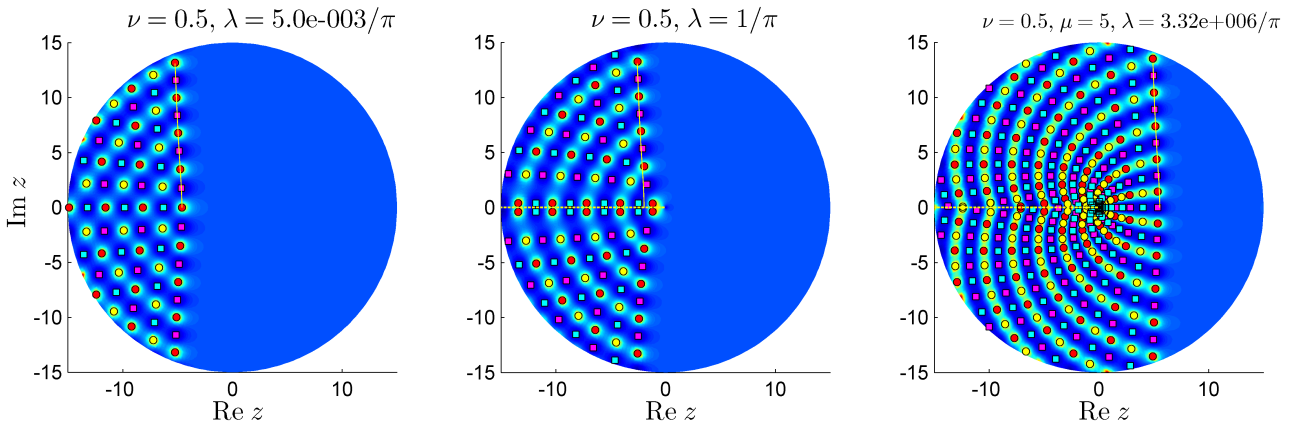


Figure 2: The typical evolution of an MTW solution with  $\nu > -\frac{1}{2}$  on the 0th sheet as  $\lambda$  is increased. The bottom left frame of Figure 1 is also a member of this sequence, slotting between the second and third frames.

We emphasize that, unlike the creation of an infinity of zeros (for  $\lambda > 1/\pi$ ) or poles (for  $\lambda < -1/\pi$ ) on  $\mathbb{R}^+$ , the profusion of poles away from  $\mathbb{R}^+$  in the stage  $\lambda > 1/\pi$  is not due to any pole creation process. Rather, as we shall observe in Figure 15, these are poles from sheets neighboring the 0th sheet that move through the branch cut as the pole density on these sheets rapidly increases for  $\lambda > 1/\pi$ .

For solutions with  $\nu \geq 0$ , zeros appear on  $\mathbb{R}^+$  only in the **third** stage when  $\lambda > 1/\pi$ . For solutions with  $-\frac{1}{2} < \nu < 0$ , however, a single zero appears on  $\mathbb{R}^+$  for  $\lambda < 1/\pi$  in the small- $B$  limit (13) with  $n = 0$  (this zero is visible in the top-left frame of Figure 4). As we shall find in section 4.2, **poles** appear on  $\mathbb{R}^+$  in the small- $B$  limit if  $n > 0$ . These facts are consequences of (15) and (16): the boundedness of  $Bb_{2,1}$  for  $n = 0$  and the unboundedness of  $Bb_{2,1}$  for  $n > 0$  in the small- $B$  limit.

Note that the absence of a dotted line on  $\mathbb{R}^-$  of the leftmost frame in Figure 2 indicates the absence of a branch cut and thus a single-valued solution. **However, this solution cannot be exactly single-valued since it would require  $\sigma = 0$  in (8) but  $\lambda \neq 0$  and thus  $\sigma \neq 0$ . However, due to limited numerical accuracy, the branch cut of the computed solution is not resolved.**

Since the solution in the upper and lower half-planes are complex conjugates for real parameters, a single-valued solution is real-valued on  $\mathbb{R}^-$ . **If a  $P_{\text{III}}$  solution with real parameters has a pole or a zero on  $\mathbb{R}^-$ , then the solution is real-valued on  $\mathbb{R}^-$  within the radius of convergence of the Laurent or Taylor expansion about the pole or zero since all the Laurent or Taylor coefficients are real-valued. Hence, the presence of poles and zeros close to  $\mathbb{R}^-$  in the left frame of Figure 2 indicates that the solution is nearly single-valued.**

We have found that solutions with half-integer  $\nu$ -values are the only solutions that are **nearly** single-valued during the first stage when  $0 < \lambda \leq \lambda_c$ , with poles and zeros **close to** the negative real axis. When  $\lambda$  exceeds  $\lambda_c$ , the poles and zeros on  $\mathbb{R}^-$  ‘split’ **in which case  $\mathbb{R}^-$  is unambiguously a branch cut**, as shown in the middle frame in Figure 2. Solutions for which  $\nu$  is not a half-integer are multivalued for all  $\lambda > 0$ , with poles and zeros above and below the branch cut. We shall observe a similar phenomenon again in Figure 6, where solutions with (approximate) negative half-integer  $\nu$ -values are **nearly** single-valued for  $0 < \lambda \leq \lambda_c$ , with poles close to  $\mathbb{R}^-$ , while the other solutions are multivalued for all  $\lambda > 0$ . In section 5.2, we shall discuss one-parameter families of solutions with negative half-integer  $\nu$ -values that are related to the MTW solutions and that are **exactly** single-valued **for all values of the arbitrary parameter**. **The small- $z$  (8) or large- $z$  (5) expansions give no indication why it should be that MTW solutions with half-integer  $\nu$  values are nearly single-valued for small  $\lambda$ . In particular,  $\sigma = \sigma(\lambda)$  in (11), which determines the type of branch point at  $z = 0$ , is independent of  $\nu$ .**

### 3.1.1 Pole-free regions

The distinctive feature of the MTW solutions is their pole-free regions in the right half-plane. It follows from (5) that the entire right half-plane is pole free as  $z \rightarrow \infty$ . However, as Figure 2 illustrates, there may be poles in the finite right half-plane and the pole-free region varies significantly as a function of the parameters. The dependence of the pole-free regions on the parameters can be understood intuitively and analytically by considering only the second term of the asymptotic expansion (5):

$$m(z; \nu, \lambda) = \lambda 2^{-2\nu} \Gamma\left(\nu + \frac{1}{2}\right) z^{-\nu-1/2} e^{-2z}. \quad (24)$$

This is based on the observation, which follows from (5), that a  $\mathcal{O}(m(z; \nu, \lambda)/z)$  approximation to the solution can be constructed by considering only  $m(z; \nu, \lambda)$ :

$$1 + m(z; \nu, \lambda) = u(z; \nu, \lambda) + \mathcal{O}\left(\frac{m(z; \nu, \lambda)}{z}\right), \quad z \rightarrow \infty, \quad -\frac{\pi}{2} < \arg z < \frac{\pi}{2}. \quad (25)$$

On the region  $|\theta| > \frac{\pi}{2}$ , the error of the estimate (25) becomes unbounded as  $z \rightarrow \infty$ . However, we shall find that in the finite plane, the estimates derived from (25) can also be reasonably accurate in the left half-plane.

If, as in Figure 2,  $\nu$  is fixed and  $\lambda$  is scaled by  $e^{2t}$ ,  $t \in \mathbb{R}$ , then

$$\begin{aligned} m(z; \nu, e^{2t}\lambda) &= \lambda 2^{-2\nu} \Gamma\left(\nu + \frac{1}{2}\right) z^{-\nu-1/2} e^{-2(z-t)} = \left(\frac{z}{z-t}\right)^{-\nu-1/2} m(z-t; \nu, k), \\ &= \left(1 - \frac{t}{z}\right)^{\nu+1/2} m(z-t; \nu, k), \\ &= m(z-t; \nu, k) + \mathcal{O}\left(\frac{t}{z}\right), \quad |z| \gg |t|. \end{aligned} \quad (26)$$

We conclude from (26) and (25) that the pole-free region is displaced horizontally by approximately  $t$  units if  $\lambda$  is scaled by  $e^{2t}$  and this approximation improves as  $|z|$  increases. Hence, the approximate horizontal displacements from the left to the middle frame and from the middle frame to the right frame in Figure 2 are, respectively,

$$t = \frac{1}{2} \log\left(\frac{1}{5 \times 10^{-3}}\right) \approx 2.65 \quad \text{and} \quad t = \frac{1}{2} \log(\cosh(5\pi)) \approx 7.51. \quad (27)$$

To test these estimates, we construct an interpolant through the poles and zeros on the boundary of the pole-free region in the upper half-plane of the solution in the left column of Figure 2, which is indicated by a yellow curve. Then we translate the interpolant horizontally to the right by the amounts in (27) (these interpolants are also shown in Figure 2) and measure the horizontal differences between the translated interpolants and the poles and zeros on the boundaries of the pole-free regions. The horizontal differences are shown in Figure 3. As expected from (26), the accuracy of the estimated horizontal displacements improves with  $|z|$ . Furthermore, the errors in Figure 3 confirm the remark above, viz. that reasonable estimates can be derived from (25) even if the boundary of the pole-free region is in the left half-plane, as in the left column of Figure 2.

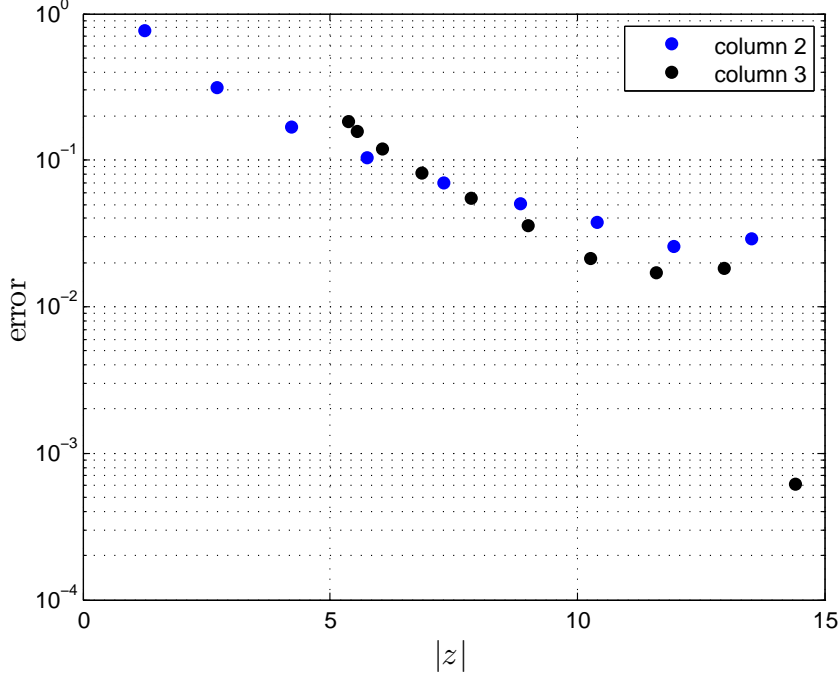


Figure 3: The error of the estimates (27) of the horizontal displacements of the pole-free regions in the second and third columns of Figure 2. Each dot represents the difference between the real part of a pole or zero on the boundary of the pole-free region in the second or third column of Figure 2 and the yellow curve in that column.

### 3.2 Fixed $\lambda$ , varying $\nu$

In Figure 4,  $\lambda$  is fixed and as  $\nu > -\frac{1}{2}$  increases, the angular widths of the pole-free regions in the finite plane increase. Specifically, let  $z^*$  be the location of the outermost pole or zero on the boundary of the pole-free region in the upper half-plane of a solution in Figure 4;  $z^*$  is indicated by a yellow open circle in the top-left and bottom-right frames of Figure 4. For the  $\nu = -\frac{1}{4}$  (top-left frame) and  $\nu = \frac{3}{2}$  (bottom-right frame) solutions,  $\arg z^* = 0.51\pi$  and  $\arg z^* = 0.60\pi$ , respectively, which is an angular displacement of  $0.09\pi$ .

To estimate the angular displacement of the pole-free regions between the frames in Figure 4, we find the angular displacement of the modulus of  $m(z; \nu, \lambda)$ , for fixed  $\lambda$  and a change in  $\nu$  of  $c$ , by solving the following equation for  $\delta$ :

$$\frac{|m(re^{i(\theta+\delta)}; \nu + c, \lambda)|}{|m(re^{i\theta}; \nu, \lambda)|} = 2^{-2c} \left| \frac{\Gamma(\nu + \frac{1}{2} + c)}{\Gamma(\nu + \frac{1}{2})} \right| r^{-c} \exp[-2r(\cos(\theta + \delta) - \cos \theta)] = 1.$$

We find that

$$\delta = \delta(r, \theta, \nu, c) = \cos^{-1} \left\{ -\frac{1}{2r} \log \left[ (4r)^c \left| \frac{\Gamma(\nu + \frac{1}{2})}{\Gamma(\nu + \frac{1}{2} + c)} \right| \right] + \cos \theta \right\} - \theta, \quad \theta \in [0, \pi]. \quad (28)$$

Due to the up-down symmetry of the modulus of the MTW solutions with real parameters, it is sufficient to consider  $\theta \geq 0$  in (28). In the limit  $r \rightarrow \infty$ , it follows from (25) that (28) is a valid estimate for the angular displacement of the pole-free regions only if  $-\frac{\pi}{2} < \theta < \frac{\pi}{2}$ ; in this limit there is no angular displacement,

$$\lim_{r \rightarrow \infty} \delta(r, \theta, \nu, c) = 0, \quad 0 \leq \theta < \frac{\pi}{2}, \quad \nu, \nu + c \neq -\frac{1}{2} - n, \quad n \geq 0.$$

In the finite plane, we shall estimate the angular displacement of the pole-free regions using (28), not only in the right half-plane but also in the left half-plane. Close to the imaginary axis, i.e., for  $\theta = \frac{\pi}{2} - \epsilon$  with  $0 \leq |\epsilon| \ll 1$ , (28) can be simplified to

$$\delta \approx \frac{1}{2r} \log \left[ (4r)^c \left| \frac{\Gamma(\nu + \frac{1}{2})}{\Gamma(\nu + \frac{1}{2} + c)} \right| \right], \quad \theta = \frac{\pi}{2} - \epsilon, \quad 0 \leq |\epsilon| \ll 1. \quad (29)$$

and if  $\theta = \frac{\pi}{2}$ , then (28) becomes

$$\delta = \sin^{-1} \left\{ \frac{1}{2r} \log \left[ (4r)^c \left| \frac{\Gamma(\nu + \frac{1}{2})}{\Gamma(\nu + \frac{1}{2} + c)} \right| \right] \right\}, \quad \theta = \frac{\pi}{2}.$$

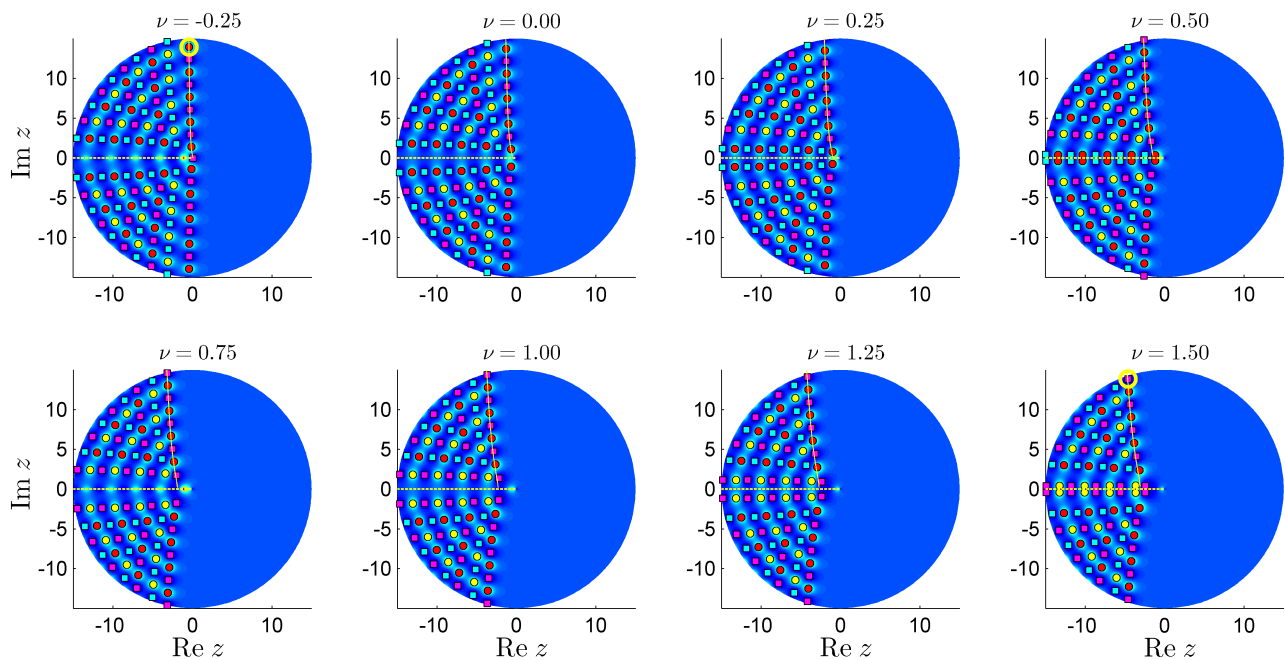


Figure 4: The typical variations between MTW solutions with  $\nu > -\frac{1}{2}$  and a fixed  $\lambda$  ( $\lambda = 1/\pi$  in this case). Note the slight differences in the pole fields close to the branch cut and how the angular width of the pole-free region increases with  $\nu$ . The second solution in the top row ( $\nu = 0$ ,  $\lambda = 1/\pi$ ) is related to the correlation function of the 2D Ising model [25, 37].

To test the estimate (28), we construct an interpolant through the poles and zeros on the boundary of the pole-free region in the top-left frame of Figure 4, which is shown as a yellow curve. Then we displace angularly every point of the interpolant by  $\delta(r, \theta, \nu, c)$ , defined in (28), to obtain the approximate pole-free boundary in row 1, column 2 of Figure 4. This angularly displaced interpolant is then displaced angularly again, according to (28), to obtain the approximate pole-free boundary in row 1, column 3 of Figure 4. This is repeated to obtain the remaining approximate pole-free boundaries in Figure 4.

Figure 5 shows plots of the angular displacements (28), in blue, and the approximate angular displacements (29), in red, for the solutions in the corresponding rows and columns of Figure 4. The errors in the final frame of Figure 5 are obtained by measuring the differences between the real parts of the poles and zeros on the boundaries of the pole-free regions and the angularly displaced interpolants. Figure 5 confirms the expectation from Figure 4: that the estimated angular displacements of the pole-free regions are positive and decrease monotonically for sufficiently large  $r$ .

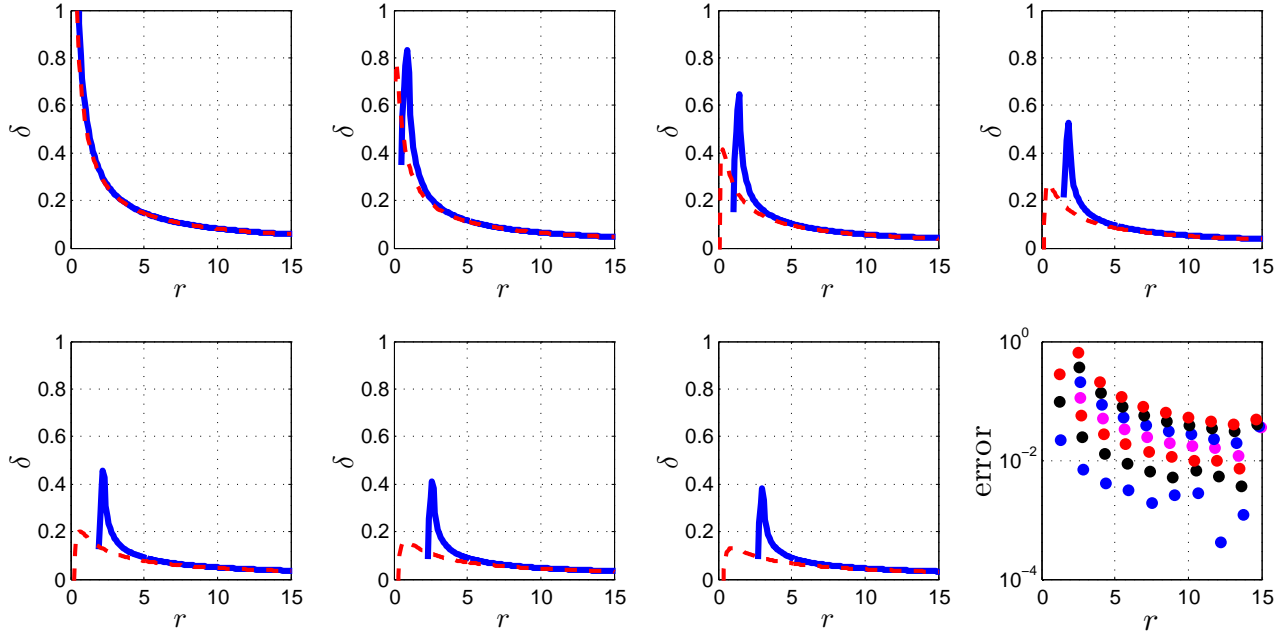


Figure 5: The angular displacements (28) (blue) of the estimated boundaries of the pole-free regions of the solutions in the corresponding rows and columns of Figure 4, as well as the approximate angular displacement (29) (red). The error of the estimated boundaries increases from frame to frame. Hence, the bottom row of dots in the bottom-right frame are the errors for the estimated pole-free boundary of the solution in row 1, column 2 of Figure 4 and the top row of dots are for the solution in row 2, column 4 of Figure 4.

## 4 MTW solutions with $\nu < -\frac{1}{2}$ on the 0th sheet

For the MTW solutions with  $\nu < -\frac{1}{2}$ , the large- $z$  formula and the small- $z$  formulas are discontinuous functions of the parameters; see (2) with  $\nu = -\frac{1}{2} - n$ ,  $n \geq 0$ , (13), (14) and (19). However, we shall find that except for transitions through the critical parameter values, the pole dynamics of the MTW solutions with  $\nu < -\frac{1}{2}$  are similar to those with  $\nu > -\frac{1}{2}$ .

### 4.1 $\sigma < \sigma_c$

As for the MTW solutions with  $\nu > -\frac{1}{2}$ , a pole field moves horizontally to the right from the left half-plane as  $\sigma$  (or  $\lambda$ , see (11)) is increased from zero. Figure 6 shows pole fields with  $\sigma < \sigma_c$ , where  $\sigma_c$  is defined in (13) and (14). We observe that  $2[-\nu] + 1$  rows of poles are dislodged from the pole field on the left when  $\nu \approx -\frac{1}{2} - n$  and that these rows of poles undergo a reciprocal transformation when  $\nu$  transitions through the critical value  $-\frac{1}{2} - n$ . This can be ascribed to the sign change of the gamma function in the large- $z$  formula (5) during this transition. **As  $\nu$  decreases in Figure 6, poles and zeros emerge through the branch cut and there are changes in the angular widths of the pole-free regions that can be quantified using (28).**

**The first six solutions in Figure 6 have a fixed value of  $\sigma$  (and thus of  $\lambda$ ) and the final six solutions in Figure 6 have a different fixed value of  $\lambda$ . Hence, we apply the formula (28), for the angular displacements of the estimated pole-free boundaries, separately to the two sets of six solutions in Figure 6. The resulting angular displacements are shown in Figure 7, in blue, along with the approximate angular displacements (29), in red, as well as the errors of**

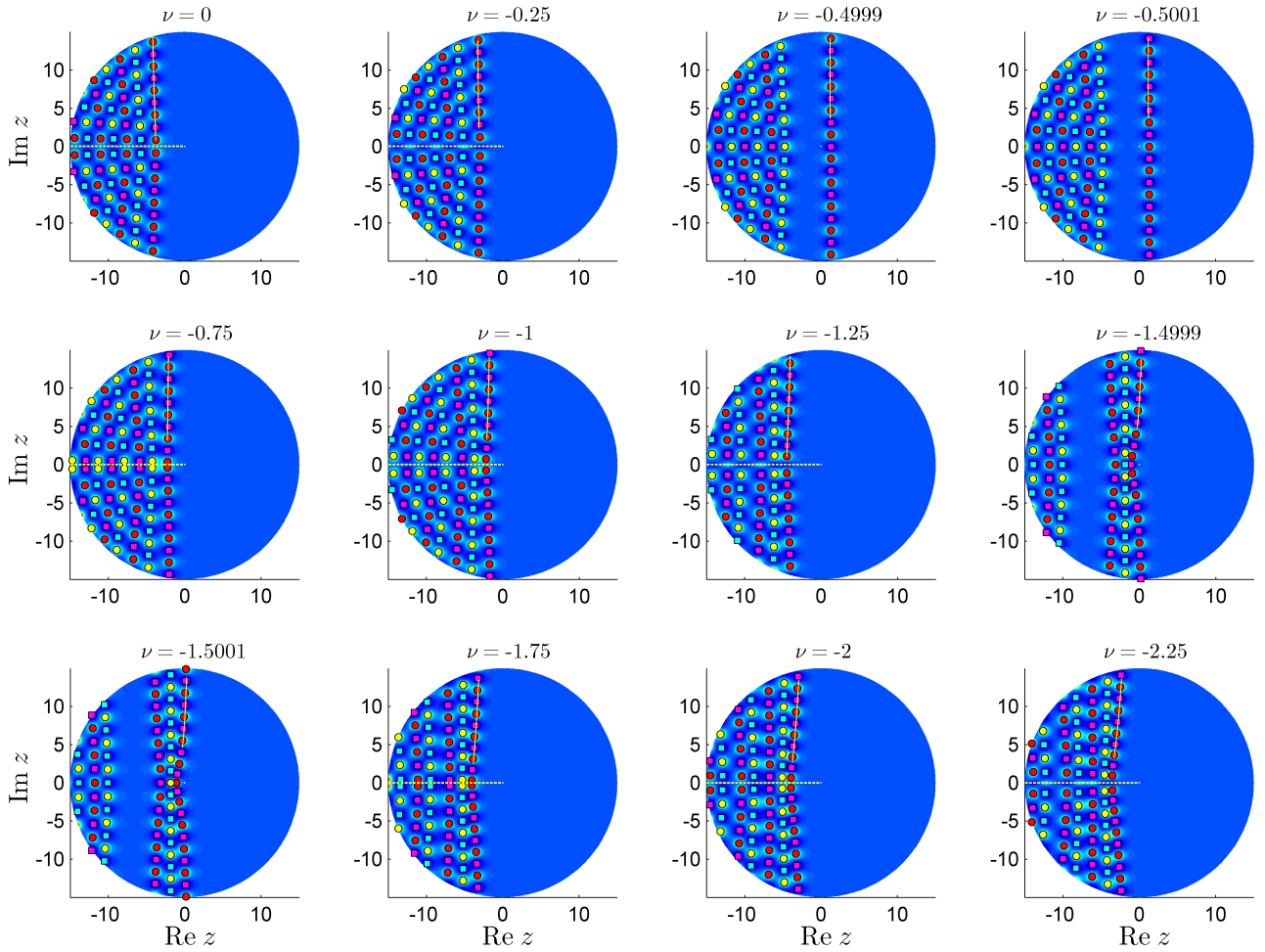


Figure 6: The pole dynamics of MTW solutions with  $\nu < -\frac{1}{2}$  preceding the approach of the critical  $\sigma$  value, i.e.,  $\sigma < \sigma_c$ . The solutions with  $0 \leq \nu \leq -1$  and  $\nu < -1$  have the parameter values  $\sigma = 4.8 \cdot 10^{-5}$  and  $\sigma = 4.8 \cdot 10^{-6}$ , respectively.

the estimated pole-free boundaries. Except for the solutions in the top-right and bottom-left frames of Figure 6, the angular displacements of the pole-free boundaries are negative as  $\nu$  decreases between frames (in Figure 4 the angular displacements are positive but  $\nu$  increases between frames). Note that different vertical scales are used in Figure 7.

## 4.2 $\sigma \rightarrow \sigma_c$

### 4.2.1 Numerical observations

As  $\sigma$  is increased from the small values in the caption of Figure 6, the rightward horizontal movement of the pole fields is continued. As  $\sigma$  increases through the critical value  $\sigma_c$ , a finite number of poles appear on  $\mathbb{R}^+$  in the  $z$ -plane, which corresponds to  $\mathbb{R}$  in the  $\zeta$ -plane. Figure 8 shows the transition through  $\sigma_c$  in the  $\zeta$ -plane for three of the solutions in Figure 6. The first row of Figure 8 shows a solution in the small- $B$  limit (13) with  $n = 1$ ; the second row shows a solution in the large- $B$  limit (14) with  $n = 1$  and the third row shows a solution with the critical parameter value (19) with  $n = 2$  (which is a special case of the large- $B$  limit (14) with  $n = 1$  and  $\nu \rightarrow -2$ ).

In the left half-plane we find that as  $\sigma \rightarrow \sigma_c^-$  (left column of Figure 8) poles and zeros are equally spaced along vertical lines. The vertical spacing between the two pairs of zeros (first row) or poles (second and third rows) is  $2\pi/|\nu + 1|$  and the spacing between the single vertical

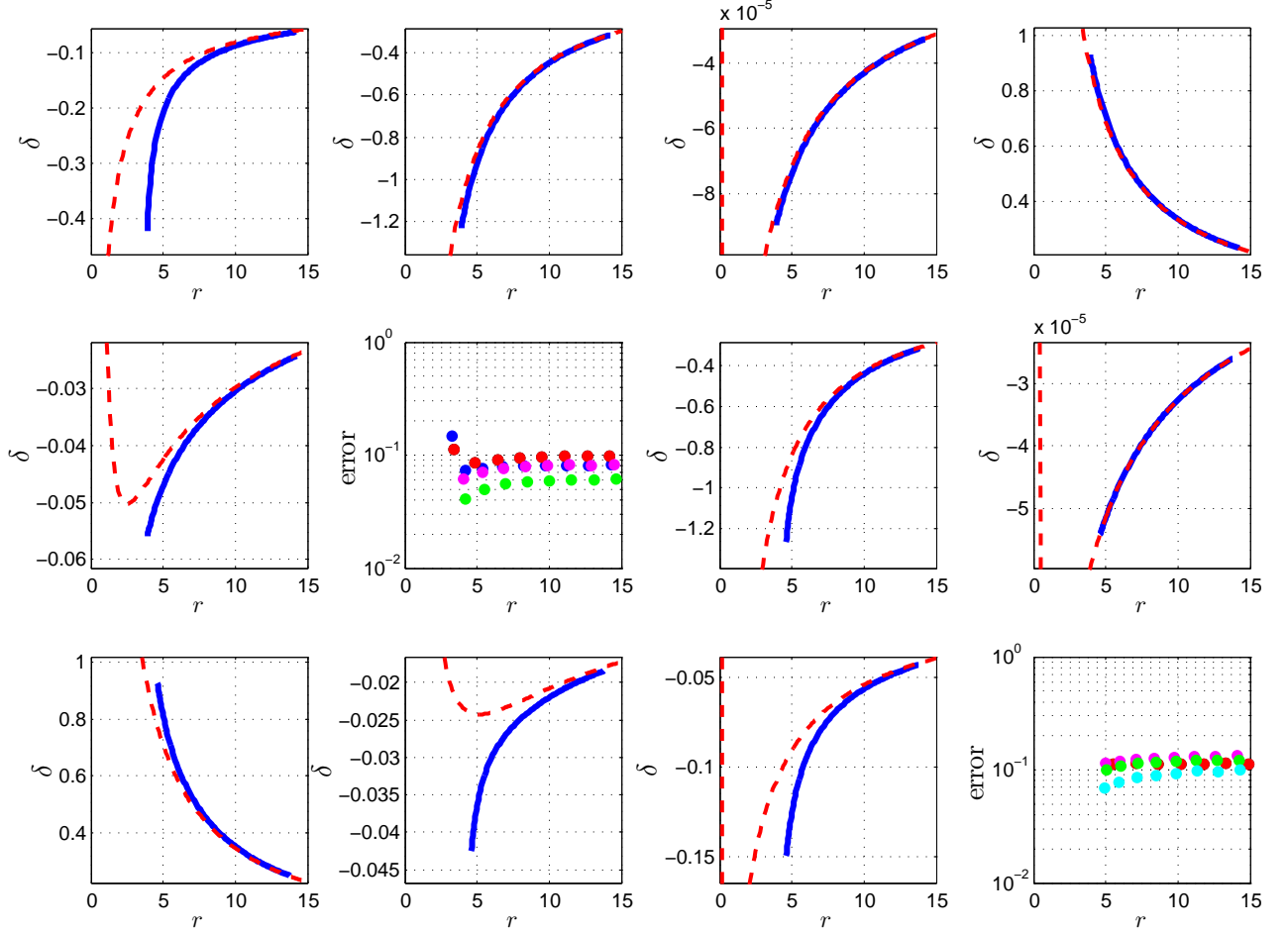


Figure 7: The angular displacements (28) (blue) of the estimated pole-free boundaries of the solutions in the corresponding rows and columns of Figure 6 along with the approximate angular displacement (29) (red). The errors (shown in row 2, column 2 and row 3, column 4) of the two sets of five angularly displaced estimated pole-free boundaries show that the yellow curves in Figure 6 are reasonable estimates of the actual pole-free boundaries.

row of four poles (first row) or four zeros (second and third rows) is  $2\pi/|\nu|$ . Furthermore, the spacing is symmetric about  $\text{Im } \zeta = 0$ . Thus, the pairs of zeros or poles and the single vertical row of poles or zeros are at, respectively,

$$\zeta = x_1 + \frac{(2k+1)\pi i}{\nu+1} \quad \text{and} \quad \zeta = x_2 + \frac{(2k+1)\pi i}{\nu}, \quad k \in \mathbb{Z}, \quad (30)$$

where  $x_1$  and  $x_2$  depend on  $\sigma$  and  $x_1 < x_2 < 0$ . Figure 8 shows the solution on the 0th sheet ( $|\text{Im } \zeta| \leq 2\pi$ ), but we have found that the spacing (30) holds on all the sheets ( $|\text{Im } \zeta| > 2\pi$ ).

As  $\sigma \rightarrow \sigma_c^-$ , the poles and zeros move infinitely far into the left half-plane,  $x_1 < x_2 \rightarrow -\infty$  in (30). As  $\sigma$  increases through  $\sigma_c$ , the poles and zeros return from  $\text{Re } \zeta = -\infty$  along

$$\zeta = x_1 + \frac{2k\pi i}{\nu+1} \quad \text{and} \quad \zeta = x_2 + \frac{2k\pi i}{\nu}, \quad k \in \mathbb{Z}, \quad (31)$$

where  $x_1 < x_2$ , see the second column of Figure 8. In the  $z$ -plane (recall  $z = e^{\zeta/2}$ ), the movement of the poles and zeros from (30) to (31) corresponds to a rotation through  $\pi/(2\nu+2)$

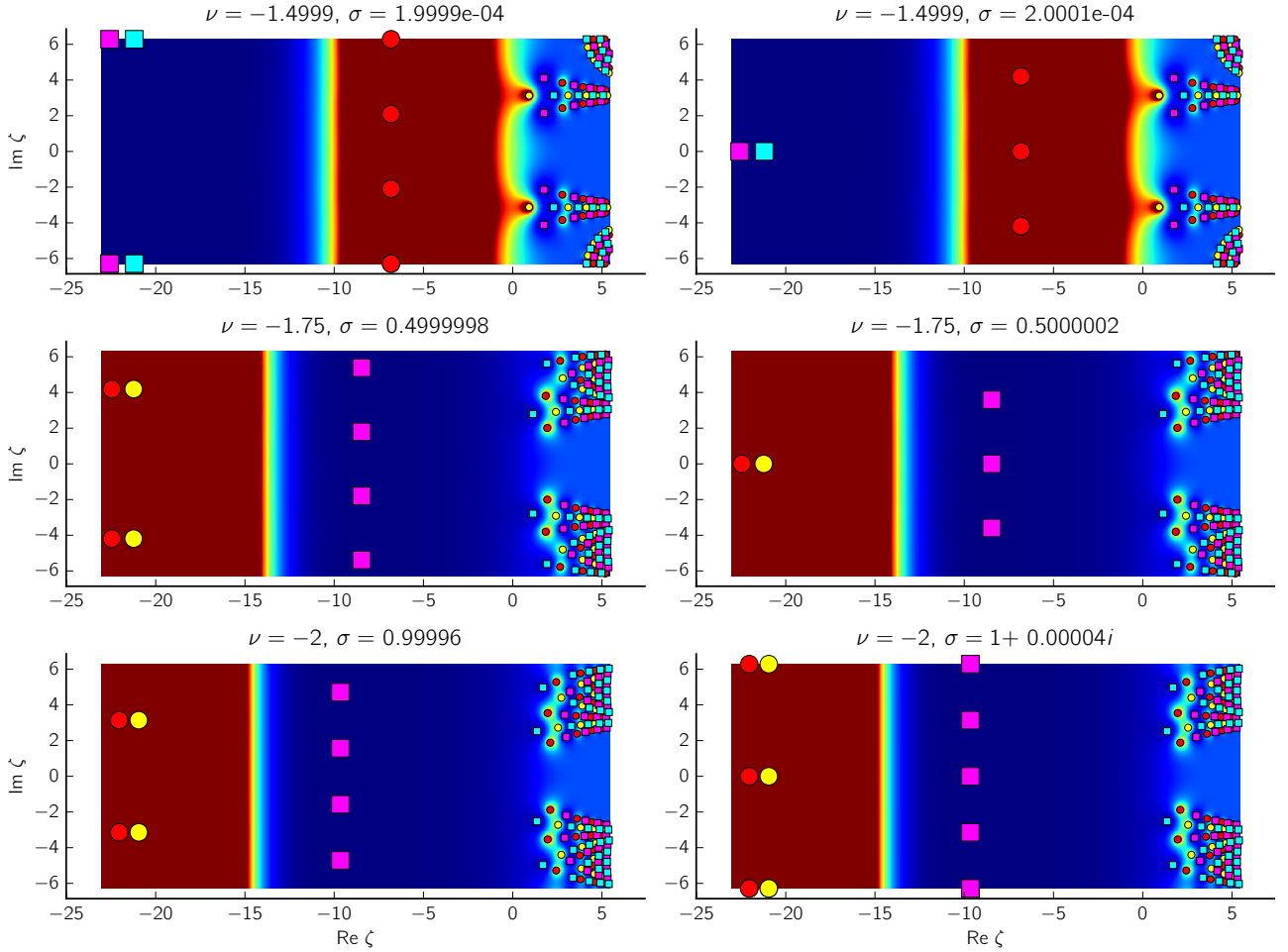


Figure 8: Round( $-\nu$ ) poles appear on  $\mathbb{R}^+$  in the  $z$ -plane, or  $\mathbb{R}$  in the  $\zeta$ -plane, as  $\sigma$  increases through  $\sigma_c$ , defined in (13) and (14).

(mod  $2\pi$ ) and  $\pi/(2\nu)$  (mod  $2\pi$ ). The appearance of poles and zeros on  $\text{Im } \zeta = 0$  as  $\sigma$  increases through  $\sigma_c$ , see (31) with  $k = 0$ , corresponds to the appearance of poles and zeros on  $\mathbb{R}^+$  in the  $z$ -plane.

In Figure 8 there is no perceptible change in the pole fields in the right half-plane as  $\sigma$  transitions through  $\sigma_c$ . This is to be expected since the large- $z$  formula (5), unlike the small- $z$  formulae (9)–(12), is a continuous function of the parameters in the limit  $\sigma \rightarrow \sigma_c$  for fixed  $\nu$ .

Our numerical solutions indicate that the observations in (30) and (31) generalize as follows in the small- $B$  (13) and large- $B$  (14) limits. In the limit  $\sigma \rightarrow \sigma_c^-$  there are pairs of zeros (in the small- $B$  limit) or poles (in the large- $B$  limit) at

$$\zeta = x_1 + \frac{(2k+1)\pi i}{\nu+n}, \quad \zeta = x_3 + \frac{(2k+1)\pi i}{\nu+n-2}, \dots, \zeta = x_{2\lceil n/2 \rceil - 1} + \frac{(2k+1)\pi i}{\nu+n+2-2\lceil n/2 \rceil}, \quad (32)$$

and there are pairs of poles (in the small- $B$  limit) or zeros (in the large- $B$  limit) at

$$\zeta = x_2 + \frac{(2k+1)\pi i}{\nu+n-1}, \quad \zeta = x_4 + \frac{(2k+1)\pi i}{\nu+n-3}, \dots, \zeta = x_{2\lceil (n-1)/2 \rceil} + \frac{(2k+1)\pi i}{\nu+n+1-2\lceil (n-1)/2 \rceil} \quad (33)$$

where  $k \in \mathbb{Z}$ . If  $n$  is odd, as in Figure 8, there is a single vertical row of poles (in the small- $B$  limit) or zeros (in the large- $B$  limit) at

$$\zeta = x_{n+1} + \frac{(2k+1)\pi i}{\nu}, \quad k \in \mathbb{Z}, \quad (34)$$

where  $x_1 < \dots < x_{n+1} < 0$ . If  $n$  is even, there is a single vertical row of zeros (in the small- $B$  limit) or poles (in the large- $B$  limit) at the points in (34). As in Figure 8, if  $\sigma \rightarrow \sigma_c^-$ , then  $x_1 < \dots < x_{n+1} \rightarrow -\infty$  and if  $\sigma \rightarrow \sigma_c^+$ , then the poles and zeros return from  $\text{Re } \zeta = -\infty$  and the points at which they reside are as in (32), (33) and (34), except that  $(2k+1)$  is replaced by  $2k$ . The upshot of this is that round( $-\nu$ ) poles appear on  $\mathbb{R}^+$  in the  $z$ -plane as  $\sigma$  increases through  $\sigma_c$  in the small- $B$  and large- $B$  limits.

#### 4.2.2 Theoretical observations

We now attempt to reconcile the observations above with the small- $z$  formulae (9)–(12). We confine our attention to the positive real axis,  $z = x > 0$ , or, equivalently, the real  $\zeta$ -axis. Starting with the observations: it follows from (32), (33) and (34) that if  $\sigma \rightarrow \sigma_c^-$ , then there are no poles or zeros on the real  $\zeta$ -axis, see also the left column of Figure 8. Since the large- $z$  formula (5) is strictly positive on  $\mathbb{R}^+$ , we conclude that if  $\sigma \rightarrow \sigma_c^-$ , then the solution is strictly positive on  $\mathbb{R}^+$ . Only when  $\sigma > \sigma_c$  do poles or zeros appear on the real  $\zeta$ -axis (see right column of Figure 8). Thus, if  $\sigma > \sigma_c$ , then the solution changes sign on  $\mathbb{R}^+$ .

We now consider the small- $z$  expansion (9) on the positive real axis. For  $\sigma_c$  defined in (13) and (14),

$$\sigma < \sigma_c \Rightarrow B(\sigma, \nu) > 0 \quad \text{and} \quad \sigma > \sigma_c \Rightarrow B(\sigma, \nu) < 0. \quad (35)$$

Thus, if  $\sigma \rightarrow \sigma_c^-$ , then the first two terms of (9),  $Bx^\sigma$  and  $Bb_{1,1}x$  (see (10)), the dominant terms in the limit  $x \rightarrow 0^+$ , are strictly positive, which is consistent with the observations above. In the large- $B$  limit (14) with  $\sigma \rightarrow \sigma_c^+$ , we deduce from (35) that the leading order term,  $Bx^\sigma$ , is negative, with  $B$  arbitrarily large negative, while the large- $x$  formula is positive. This is consistent with the presence of at least one pole on the real  $\zeta$ -axis, see the second and third rows in the right column of Figure 8. In the small- $B$  limit (13) with  $\sigma \rightarrow \sigma_c^+$ , the first term of (9) is negative; the second term is positive; the third term,  $Bb_{1,2}x^{1+2\sigma}$ , is negative but negligible, see (10), and the fourth term,  $Bb_{2,1}x^{2-\sigma}$ , is negative and bounded if  $n = 0$ , see (15), and negative but unbounded if  $n > 0$ , see (16). This indicates the presence of at most two zeros and, if  $n > 0$ , one pole on  $\mathbb{R}^+$  in the limit  $x \rightarrow 0^+$ . This is consistent with the observations in (32), (33) and (34) (with  $(2k+1)$  replaced by  $2k$ ) according to which a pair of zeros appears on  $\text{Im } \zeta = 0$  if  $n > 0$  and at least one pole appears on  $\text{Im } \zeta = 0$  if  $n > 0$  in the small- $B$  limit (as in the right column of the first row of Figure 8).

Suppose  $\nu = -n - \frac{\ell}{2m}$ , where  $n, \ell$  and  $m$  are non-negative integers,  $\ell$  and  $m$  are relatively prime and  $\nu = -n - \frac{\ell}{2m} \neq -n - \frac{1}{2}$ . Then  $\sigma_c = (m - \ell)/m$  if  $0 < \frac{\ell}{2m} < \frac{1}{2}$  (see (13)), and  $\sigma_c = (\ell - m)/m$  if  $\frac{1}{2} < \frac{\ell}{2m} \leq 1$  (see (14) and the comment below (19)). This implies that if  $\sigma \approx \sigma_c$ , then the small- $z$  formula (9) is approximately an expansion in powers of  $1/m$  and thus the solution behavior in the limit  $z \rightarrow 0$  is approximately that of an  $m$ -branched solution. If the solution has  $m$  distinct branches in the limit  $z \rightarrow 0$ , or equivalently,  $\text{Re } \zeta \rightarrow -\infty$ , then the positions of the poles and zeros close to  $z = 0$  should repeat every  $m$  branches. That is, the sequences (32), (33) and (34) should be  $4\pi m$ -periodic in the imaginary direction, which is indeed the case<sup>6</sup>. For example, in Figure 8 we have, in the first to third rows, respectively,  $m \approx 1$ ,  $m = 2$  and  $m = 1$ . Thus, the positions of the poles and zeros are  $4\pi$ -periodic in the vertical direction in the first and third rows and  $8\pi$ -periodic in the second row, which is also evident in (30) and (31). Recalling that a pole or zero on the lines  $\text{Im } \zeta = \pm 2\pi$  correspond to a single pole or zero on  $\mathbb{R}^-$  in the  $z$ -plane since  $z = e^{\zeta/2}$ , we find that the number of poles and zeros in the left half-plane is conserved in the first and third rows of Figure 8 (for example, three poles in the left and right columns of the first row) but not in the second row. This is

<sup>6</sup>If  $\nu < 0$  is irrational so that  $\nu \neq -n - \frac{\ell}{2m}$ , then the solution has infinitely many distinct branches in the limit  $z \rightarrow 0$  and thus the pole and zero positions are not periodic in the vertical direction.

because  $m = 1$  in the first and third rows and  $m = 2$  in the second row. However, if one counts the number of poles and zeros in the left half-plane in the second row on  $m = 2$  sheets, e.g., on  $-2\pi < \text{Im } \zeta \leq 6\pi$ , then the number of poles and zeros are conserved.

In the limit  $\sigma \rightarrow \sigma_c$ , the poles and zeros at (32), (33) and (34) move infinitely far into the left half-plane,  $x_1 < \dots < x_{n+1} \rightarrow -\infty$ , which implies that the poles and zeros coalesce in the limit at  $z = 0$ . Since the pairs of poles and zeros have residues and derivative values, respectively, of opposite signs (see Figure 8) they effectively cancel in the limit when they coalesce. This leaves the single vertical row of poles or zeros at (34) that coalesce in the limit at  $z = 0$  but on different sheets. If a  $P_{\text{III}}$  solution with MTW parameters (1) admits a pole at  $z = 0$ , then it is a simple pole with residue  $c_{-1} = -2\nu$ , as one can confirm by substituting a Laurent expansion about  $z = 0$  into  $P_{\text{III}}$ . This is consistent with the first row of Figure 8 in which three poles with  $c_{-1} = +1$  coalesce at  $z = 0$  in the limit  $\sigma \rightarrow \sigma_c$ , resulting in a pole at  $z = 0$  with  $c_{-1} = 3 \approx -2\nu = -2(-1.4999)$ . Now, the reciprocal of an MTW solution is also an MTW solution, see (7). Thus, if an MTW solution has a simple pole with  $c_{-1} = -2\nu$  at  $z = 0$ , then the reciprocal of this solution is also an MTW solution and it has a simple zero at  $z = 0$  with  $c_1 = 1/c_{-1} = -\frac{1}{2\nu}$ . Furthermore, if  $n$  poles with  $c_{-1} = +1$  of an MTW solution coalesce at  $z = 0$  to form a pole with residue  $n$ , as in the first row of Figure 8, then the coalescence of  $n$  zeros at  $z = 0$  must result in a zero at  $z = 0$  with  $c_1 = 1/n$ . Thus, in the third row of Figure 8, in which  $\nu = -2$  and four zeros with  $c_1 = 1$  coalesce, we have  $c_1 = 1/n = 1/4$ , which is consistent with the fact that  $c_1 = -\frac{1}{2\nu}$  since  $c_1 = -\frac{1}{2\nu} = 1/4 = 1/n$ . The solution in the second row of Figure 8 has two distinct branches ( $m = 2$ ) in the limit  $z \rightarrow 0$  or  $\text{Re } \zeta \rightarrow -\infty$ , thus the positions of the poles and zeros in the left half-plane are  $8\pi$ -periodic. For this solution,  $\nu = -7/4$  and there are seven zeros on two sheets with  $c_1 = 1$  that coalesce in the limit  $\sigma \rightarrow \sigma_c$ . If we consider the reciprocal of this solution, then seven poles with  $c_{-1} = 1$  coalesce on two sheets and thus the ‘residue per sheet’ is  $7/2 = n/m$ , which is the same as the residue of a pole at  $z = 0$  on a single sheet given above, i.e.,  $c_{-1} = -2\nu = 7/2$ . Thus, if seven zeros with  $c_1 = 1$  coalesce on two sheets we have a ‘derivative value per sheet’ of  $m/n = 2/7$ , which is the same as the derivative value of a zero at  $z = 0$  on a single sheet,  $c_1 = -\frac{1}{2\nu} = 2/7$ .

One can use (34) to show that the results above generalize as follows for rational  $\nu$  values. Suppose  $\nu = -n - \frac{\ell}{2m} = -\frac{2mn+\ell}{2m}$  and consider the small- $B$  limit (13), thus  $0 < \frac{\ell}{2m} < \frac{1}{2}$ . Then  $2mn + \ell$  poles with  $c_{-1} = 1$  (if  $n$  is odd) or zeros with  $c_1 = 1$  (if  $n$  is even) coalesce on  $m$  sheets, giving a residue per sheet of  $\frac{2mn+\ell}{m} = -2\nu$  and a derivative value per sheet of  $\frac{m}{2mn+\ell} = -\frac{1}{2\nu}$ . For the large- $B$  limit (14), let  $\frac{1}{2} < \frac{\ell}{2m} \leq 1$ , then  $2mn + \ell$  zeros with  $c_1 = 1$  (if  $n$  is odd) or poles with  $c_{-1} = 1$  (if  $n$  is even) coalesce on  $m$  sheets, again giving a residue per sheet of  $\frac{2mn+\ell}{m} = -2\nu$  and a derivative value per sheet of  $\frac{m}{2mn+\ell} = -\frac{1}{2\nu}$ .

### 4.3 $|\sigma| > \sigma_c$

Figure 9 shows the typical pole dynamics of an MTW solution with  $\nu < -\frac{1}{2}$  before and after the round( $-\nu$ ) poles first appear on  $\mathbb{R}^+$ . Except for the rightmost  $2[-\nu] + 1$  rows of poles that are not aligned with the pole field on the left, the movement of the poles into the right half-plane and the accumulation of zeros on  $\mathbb{R}^+$  when  $\lambda > 1/\pi$ , or  $\sigma = 1 + 2i\mu$ ,  $\mu > 0$ , is similar to that of the MTW solutions with  $\nu > -\frac{1}{2}$  (cf. Figure 2). The bottom frame of Figure 9 illustrates that if  $\sigma > \sigma_c$ , then the small- $x$  and large- $x$  asymptotics of MTW solutions with  $\nu < -\frac{1}{2}$  are similar to those of MTW solutions with  $\nu > -\frac{1}{2}$  (cf. the bottom-right frame of Figure 1), despite the presence of poles on  $\mathbb{R}^+$  in MTW solutions with  $\nu < -\frac{1}{2}$ . This makes the MTW solutions with  $\nu < -\frac{1}{2}$  reminiscent of the quasi-Hastings–McLeod solutions of  $P_{\text{II}}$ , identified in [12]. The asymptotic behavior of quasi-Hastings–McLeod solutions at  $x \rightarrow \pm\infty$  is the same as regular Hastings–McLeod solutions, a class of tronquée  $P_{\text{II}}$  solutions, despite the presence of a finite number of poles on the real axis.

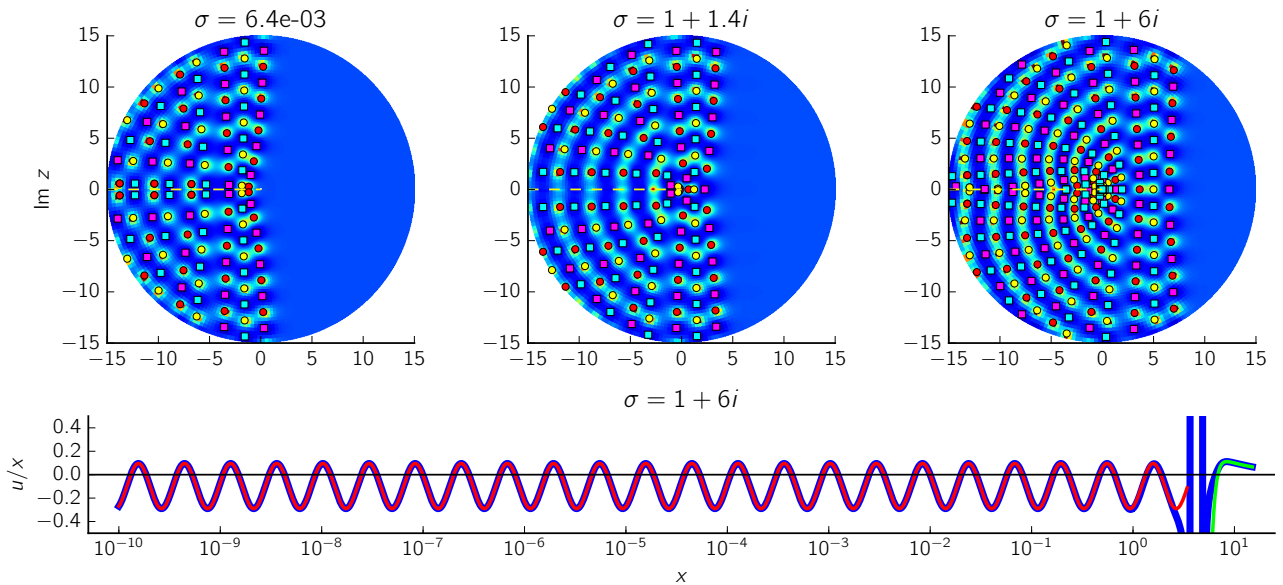


Figure 9: The pole fields of an MTW solution with  $\nu = -1.75$  before and after the round( $-\nu$ ) poles first appear on  $\mathbb{R}^+$  (see also the  $\nu = -1.75$  solution in Figures 6 and 8). The bottom frame shows the solution in the rightmost frame on  $\mathbb{R}^+$  with its small- $x$  and large- $x$  asymptotic behaviors given by (22) and (2), respectively, all divided by  $x$  (cf. the bottom-right frame of Figure 1).

## 5 Solutions with $\nu = -\frac{1}{2} - n$ on the 0th sheet

Although the MTW solutions do not exist when  $\nu = -\frac{1}{2} - n$ ,  $n \geq 0$ , since then the large- $z$  formula (2) is singular, there are two families of solutions that can be viewed as limiting MTW solutions as  $\nu \rightarrow -\frac{1}{2} - n$ . The first family satisfies only the small- $x$  MTW asymptotic formulae: (9)–(12), (17) and (22). The second family are single-valued  $P_{\text{III}}$  solutions that are expressible in terms of elementary functions and which have MTW-like large- $z$  expansions. Since each member of these families satisfies MTW asymptotic formulae only at one end of  $\mathbb{R}^+$ , we refer to the first family as the left-end MTW solutions and the second family is called the right-end MTW solutions. We denote the left-end MTW solutions by  $u(z; \nu, \sigma)$ ; thus, if  $\nu \neq -\frac{1}{2} - n$ , then  $u(z; \nu, \sigma)$  denotes an MTW solution and if  $\nu = -\frac{1}{2} - n$ , then  $u(z; \nu, \sigma)$  signifies a left-end MTW solution.

### 5.1 The left-end MTW solutions

We know from Figure 6 that for an MTW solution with  $\nu \approx -\frac{1}{2} - n$ ,  $2[-\nu] + 1$  rows of poles are dislodged from the pole field on the left. The left-end MTW solutions are the limiting cases in which these dislodged rows of poles move to  $+\infty$ , as illustrated in Figure 10. The two central frames in Figure 10 are phase portraits [36], which depict the phase of the solution  $u$ , i.e.,  $\text{Arg}(u) \in (-\pi, \pi]$ , according to the color wheel above Figure 10. Thus, the second frame shows that on the smooth regions to the left and right of the dislodged rows of poles, the solution has, respectively, negative real values, indicated by light blue, and positive real values, indicated as red. All MTW solutions asymptote to positive real values in the right half-plane as  $z \rightarrow \infty$ , see (5). However, as  $\nu$  decreases to the critical value  $-\frac{1}{2} - n$ , the dislodged poles move infinitely far to the right (thus rendering the large- $z$  formula (5) singular) resulting in negative real values in the right half-plane as  $z \rightarrow \infty$  for the left-end MTW solution, see the third frame in Figure 10. As  $\nu$  decreases through  $-\frac{1}{2} - n$ , the factor  $\Gamma(\nu + \frac{1}{2})$  in (5) discontinuously changes sign and the

dislodged poles and zeros return into the finite right half-plane as the reciprocals of poles and zeros that exited the finite right-half plane, cf. the leftmost and rightmost frames in Figure 10. In the left half-plane, however, there are no perceptible changes in the solution as  $\nu$  transitions through  $-\frac{1}{2} - n$ , see Figure 10. This is because the small- $x$  formulae (9)–(12) are continuous functions of  $\nu$  for fixed  $\sigma \neq \sigma_c$ , where  $\sigma_c$  is defined in (13) and (14).

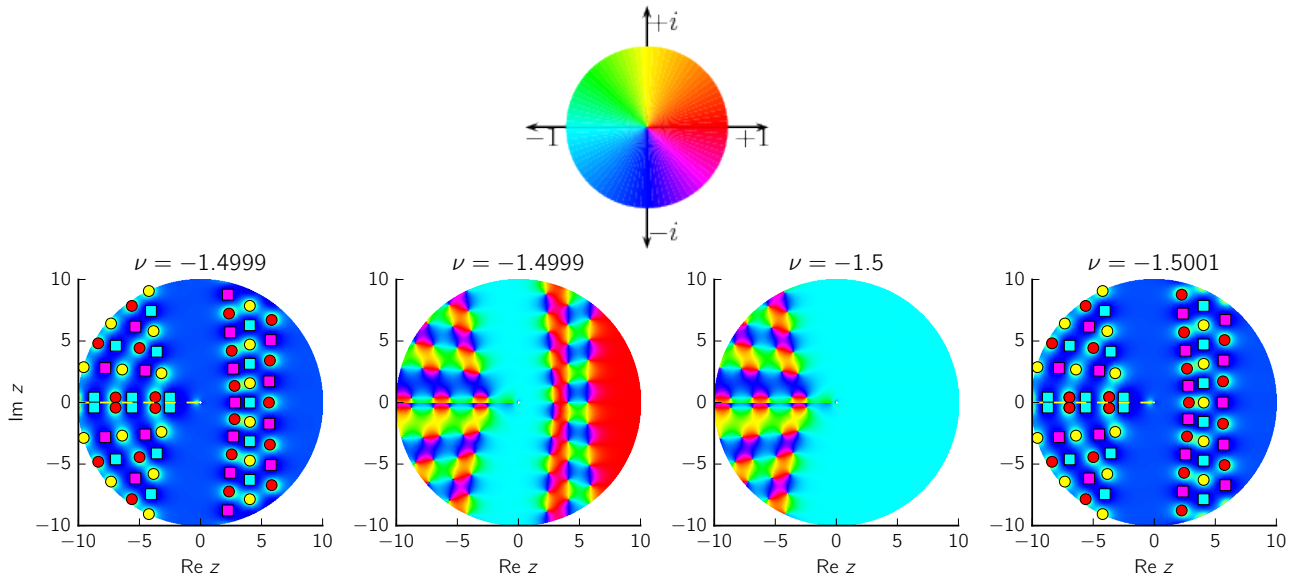


Figure 10: A left-end MTW solution (third frame) and two nearby MTW solutions: the leftmost and rightmost frames are modulus plots of the nearby MTW solutions and the second frame is a phase portrait of the solution in the leftmost frame. The only discernible differences between the solutions are in the right half-plane. For these solutions  $\sigma = 1$ . The color wheel above the figure is taken from <http://dlmf.nist.gov/help/vrml/aboutcolor>.

It is shown in Theorem 3 in the Appendix that the left-end MTW solutions,  $u(z; -\nu, \sigma)$ ,  $\nu = n + \frac{1}{2}$ ,  $n \in \mathbb{Z}$ , are the negatives of the MTW solutions  $u(z; \nu, \sigma)$ . Hence, the left-end solution in Figure 10 is the negative of the  $\nu = \frac{3}{2}$  solution in Figure 4. The large- $z$  behavior of the left-end MTW solution in Figure 10 is therefore given by the negative of the large- $z$  formula (5) and thus  $u \sim -1$ ,  $z \rightarrow \infty$  in the right half-plane.

## 5.2 The right-end MTW solutions

The  $P_{\text{III}}$  equation with  $\gamma = 1 = -\delta$  has Bessel function solutions if and only if  $\varepsilon_1\alpha + \varepsilon_2\beta = 4n + 2$ , where  $\varepsilon_1 = \pm 1$  and  $\varepsilon_2 = \pm 1$  independently and  $n \in \mathbb{Z}$  [8]. Thus, for  $P_{\text{III}}$  with MTW parameters (1), we require  $\varepsilon_1 = -\varepsilon_2$  in which case Bessel function solutions exist for  $\nu = n + \frac{1}{2}$ . It is shown in [26] that if  $\varepsilon_1 = \varepsilon_2$ , then  $P_{\text{III}}$  has solutions expressible in terms of Bessel functions of the first and second kinds while if  $\varepsilon_1 = -\varepsilon_2$ , then solutions in terms of modified Bessel functions of the first and second kinds ( $I_\alpha$  and  $K_\alpha$ , respectively) exist. For the latter case, which is applicable to solutions with MTW parameters, the modified Bessel function  $P_{\text{III}}$  solutions are [26]

$$u(z; 1 - c, -c - 1, 1, -1) = -\frac{\phi'(z)}{\phi(z)}, \quad u(z; c - 1, c + 1, 1, -1) = \frac{\phi'(z)}{\phi(z)}, \quad (36)$$

where

$$\phi(z) = C_1 z^{(1-c)/2} I_{(c-1)/2}(\pm z) + C_2 z^{(1-c)/2} K_{(c-1)/2}(\pm z),$$

and  $C_1$  and  $C_2$  are arbitrary constants. In (36),  $u(z; \alpha, \beta, \gamma, \delta)$  denotes a  $P_{\text{III}}$  solution with parameters  $\alpha, \beta, \gamma$  and  $\delta$ . The parameters in (36) are MTW parameters (1) only if  $c = 0$  in

which case the modified Bessel functions can be expressed in terms of elementary functions:  $I_{(c-1)/2}(z) = I_{-1/2}(z) = \sqrt{2/(\pi z)} \cosh z$ ,  $K_{(c-1)/2}(z) = K_{-1/2}(z) = \sqrt{\pi/(2z)} e^{-z}$ . Thus, for MTW parameters the special function solutions (36) can be expressed in terms of hyperbolic functions [26]:

$$u(z; \varepsilon, -\varepsilon, 1, -1) = -\varepsilon \frac{a \cosh z + b \sinh z}{a \sinh z + b \cosh z}, \quad \varepsilon^2 = 1. \quad (37)$$

Since we are considering solutions with  $\nu = -\frac{1}{2} - n$ ,  $n \geq 0$ , we set  $\varepsilon = -1$  in (37) which corresponds to the MTW parameter  $\nu = -\frac{1}{2}$ .

The following Bäcklund transformation maps a  $P_{\text{III}}$  solution with MTW parameter  $\nu$ , i.e.,  $u := u(z; 2\nu, -2\nu, 1, -1)$ , to a  $P_{\text{III}}$  solution with MTW parameter  $\nu \pm 1$  [26]:

$$T_\varepsilon : u(z; 2(\nu + \varepsilon), -2(\nu + \varepsilon), 1, -1) = -\frac{u(zu' + \varepsilon zu^2 + 2\nu\varepsilon u + u - \varepsilon z)}{zu' + \varepsilon zu^2 - 2\nu\varepsilon u - u - \varepsilon z}, \quad \varepsilon^2 = 1. \quad (38)$$

Hence, if we apply  $T_{-1}^n$  ( $T_{-1}^n$  denotes  $n$  applications of  $T_{-1}$ ) to the single-valued solution (37) with  $\varepsilon = -1$ , which has MTW parameter  $\nu = -\frac{1}{2}$ , we obtain a meromorphic elementary function solution with MTW parameter  $\nu = -\frac{1}{2} - n$ . We now show that these solutions can be considered as limiting MTW solutions with  $\nu \rightarrow -\frac{1}{2} - n$ .

We observe that if  $\nu = -\frac{1}{2} - n$ , then the series in the large- $z$  MTW formula (5) converges to a finite sum since then  $c_j = 0$ ,  $j \geq n + 1$  (see (6)). Thus, if we set  $\nu = -\frac{1}{2} - n$  in (5) and replace the singular factor  $\lambda \Gamma(\nu + \frac{1}{2}) 2^{-2\nu}$  with a parameter  $k$ , we obtain

$$u \sim 1 - kz^n e^{-2z} \left( 1 + \sum_{j=1}^n \frac{c_j}{z^j} \right) = 1 - kp_n(z) e^{-2z}, \quad z \rightarrow \infty, \quad -\frac{\pi}{2} < \arg z < \frac{\pi}{2}, \quad (39)$$

where  $p_n(z) = \sum_{j=0}^n c_j z^{n-j}$ . This limiting MTW large- $z$  expansion is the same as the first two leading order terms of the large- $z$  expansion of the elementary function solutions discussed above, up to a constant. For example, the solution (37) with  $\varepsilon = -1$  can be expressed as

$$u(z; -1, 1, 1, -1) = \frac{1 - \left(\frac{b-a}{a+b}\right) e^{-2z}}{1 + \left(\frac{b-a}{a+b}\right) e^{-2z}} = \frac{1 - (C/2) e^{-2z}}{1 + (C/2) e^{-2z}} = 1 - C e^{-2z} + \mathcal{O}(e^{-4z}), \quad (40)$$

for  $z \rightarrow \infty$ ,  $-\frac{\pi}{2} < \arg z < \frac{\pi}{2}$ . Since  $c_0 = 1$ ,  $p_0(z) = 1$  and thus the expansion (39) with  $n = 0$  and the first two terms of (40) match up to a constant. We show in Lemma 3 in the Appendix that the elementary function solution obtained from  $n$  applications of  $T_{-1}$  to the solution  $u(z; -1, 1, 1, -1)$  in (40) has the expansion

$$u(z; -1 - 2n, 1 + 2n, 1, -1) = T_{-1}^n u(z; -1, 1, 1, -1) = 1 - CP_n(z) e^{-2z} + \mathcal{O}(e^{-4z}), \quad (41)$$

where  $P_n(z) = \frac{(-4)^n}{n!} p_n(z)$ , for  $z \rightarrow \infty$ ,  $-\frac{\pi}{2} < \arg z < \frac{\pi}{2}$ . Hence, the two leading order terms of the limiting  $\nu \rightarrow -\frac{1}{2} - n$  MTW expansion (39) and the elementary function solution in (41) with MTW parameter  $\nu = -\frac{1}{2} - n$  match up to a scaling factor. **Moreover, if the limiting MTW expansion (39) is appropriately generalized to include the higher order exponential terms that feature in (41), then the two expansions would match to all orders, up to a scaling factor, since that expansion in powers of  $e^{-2z}$  is unique.** We therefore refer to the set of one-parameter meromorphic elementary functions defined in (41) as the right-end MTW solutions.

Figure 11 illustrates that the right-end MTW solutions are limiting MTW solutions in which the pole-fields in the left half-plane of the nearby MTW solutions move out of the finite plane. The central frame shows the single-valued right-end MTW solution (41) with  $n = 1$ , i.e.,

$$u(z; -3, 3, 1, -1) = \left( \frac{1 - (C/2) e^{-2z}}{1 + (C/2) e^{-2z}} \right) \frac{(C^2/4) e^{-4z} - 2z C e^{-2z} - 1}{(C^2/4) e^{-4z} + 2z C e^{-2z} - 1} \sim 1 - C(-4z + 1) e^{-2z}, \quad (42)$$

for  $z \rightarrow \infty$ ,  $-\frac{\pi}{2} < \arg z < \frac{\pi}{2}$ . The large- $z$  asymptotics of the nearby MTW solutions in Figure 11 are given approximately by (39) with  $p_1(z) = z - \frac{1}{4}$  (note from (42) that  $P_1(z) = \frac{(-4)^1}{1!} p_1(z)$ ),  $k = \lambda \Gamma(\nu + \frac{1}{2}) 2^{-2\nu}$  and  $\nu \approx -\frac{3}{2}$ . Thus, to (approximately) match the large- $z$  expansions of the solutions in Figure 11 we set  $C = -\lambda \Gamma(\nu + \frac{1}{2}) 2^{-2\nu} / 4$ . Since the one MTW solution in Figure 11 has  $\nu > -\frac{3}{2}$  and the other  $\nu < -\frac{3}{2}$ , the factor  $\Gamma(\nu + \frac{1}{2})$  has opposite signs for the two solutions and thus the signs of  $\lambda$  differ in Figure 11. Similar to the MTW solutions, for which  $u(z; \nu, -\lambda) = 1/u(z; \nu, \lambda)$ , see (7), it is clear from (42) that changing the sign of  $C$  yields the reciprocal solution. It is straightforward to show using (41) and (38) that this property holds for all right-end MTW solutions.

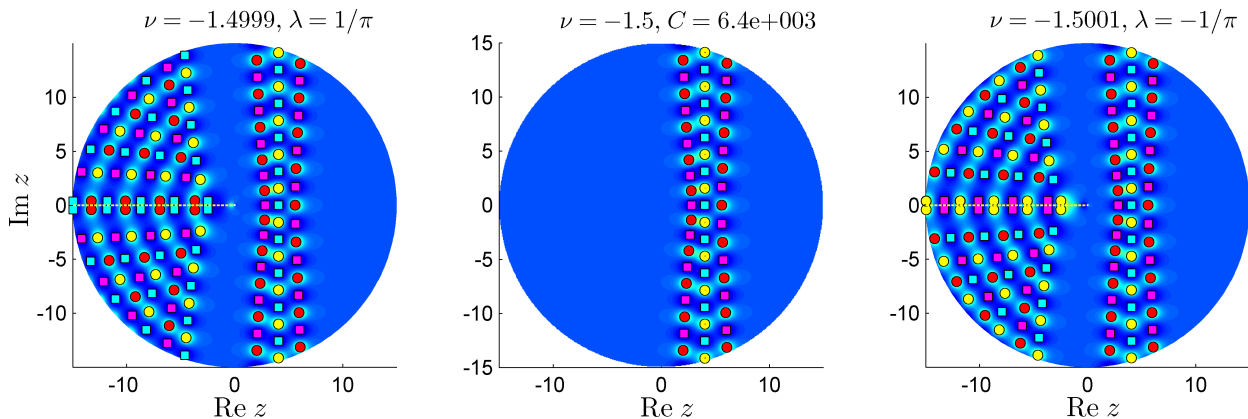


Figure 11: The single-valued right-end MTW solution, central frame, can be considered a limiting solution of its two nearby MTW solutions. As explained below (42), the parameters of the right-end MTW solution and the nearby MTW solutions,  $C$  and  $\lambda$ , respectively, are related according to  $C = -\lambda \Gamma(\nu + \frac{1}{2}) 2^{-2\nu-2}$ .

Figure 11 is analogous to Figure 10: in the latter figure the dislodged rows of poles and zeros move to  $+\infty$  and return as reciprocals whereas in Figure 11 it is the pole field in the left half-plane that moves to  $-\infty$  and returns as its reciprocal as  $\nu$  decreases through  $-\frac{1}{2} - n$ . The left-end and right-end MTW solutions constitute the limiting cases in these figures. In Figure 10 small changes in the small- $z$  formula lead to significant qualitative differences in the right half-plane. Similarly, in Figure 11, small perturbations in the right half-plane result in significant differences in the left half-planes of the solutions.

## 6 The MTW solutions on multiple sheets

The pole field dynamics of the MTW solutions on sheets other than the 0th sheet is very different for the two cases  $0 < \sigma < 1$  and  $\sigma = 1 + 2i\mu$ ,  $\mu \geq 0$ . This can be ascribed to the type of branch point admitted at  $z = 0$  in the two cases. We shall find that if  $\sigma$  is a rational number with  $0 < \sigma < 1$ , then, as suggested by the small- $z$  approximation  $u(z/2) \sim Bz^\sigma$  (see (9)),  $z = 0$  is an algebraic branch point and thus the MTW solution has a finite number of distinct branches. It is stated (but not proved) in [23] that algebraic branch points of  $P_{\text{III}}$  solutions must have order three. However, as we shall prove in Corollary 1 and as our numerical solutions confirm (e.g. Figure 13), MTW solutions with algebraic branch points of any order exist. For the case  $\sigma = 1 + 2i\mu$ ,  $\mu \geq 0$ , for which the small- $x$  approximations (17)–(22) are valid, our computations indicate that the MTW solutions have infinitely many distinct branches. The algebraic branch points admitted at  $z = 0$  for  $0 < \sigma < 1$  imply certain rotational symmetries which lead to the existence of pole-free sectors on sheets neighboring the 0th sheet that are

not present when  $\sigma = 1 + 2i\mu$ ,  $\mu \geq 0$ . Henceforth we consider only the  $s$ -th sheets with  $s > 0$  since, as we noted in section 2.3, an MTW solution with real parameters on  $\arg z < 0$  is the complex conjugate of the solution on  $\arg z > 0$ . Thus, the solution features on the  $-s$ -th sheet are easily deduced from those on the  $s$ -th sheet.

## 6.1 Empirical results for $0 < \sigma < 1$

We used our computational method to survey the MTW solutions on sheets 0–4. For fixed  $\nu$  we found that multiple pole-free sectors appear on these sheets as  $\sigma$  is varied between 0 and 1. Table 2 describes all the pole-free sectors that we found. All MTW solutions have a pole-free sector on sheet 0, contained in  $-\pi/2 < \arg z < \pi/2$ , with  $u \sim 1$ ,  $z \rightarrow \infty$ , see (5). However, a pole-free sector occurs on sheet  $s$ ,  $s > 0$ , only if  $\sigma$  is rational, i.e.,  $0 < \sigma = \frac{n_1}{n_2} < 1$ , where  $n_1$  and  $n_2$  are relatively prime. As we shall prove, it follows from the small- $z$  expansion (8) that if  $\sigma = \frac{n_1}{n_2}$ , then the solution is invariant under rotations through an angle of  $2\pi n_2$  and thus we need only consider sheets 0 to  $n_2 - 1$ , or the region  $-\pi/2 < \arg z \leq (2n_2 - \frac{1}{2})\pi$ . Table 2 shows that if  $n_1$  and  $n_2$  have opposite parity, then MTW solutions with  $\nu \in \mathbb{Z}$  have one more pole-free sector than MTW solutions with  $\nu \in \mathbb{R} \setminus \mathbb{Z}$ : a pole-free sector in a right half-plane with  $u \sim -1$  if  $n_2$  is odd, or in a left half-plane with  $u \sim 1$  if  $n_2$  is even. If  $n_1$  and  $n_2$  are both odd, then MTW solutions with  $\nu \in \mathbb{Z}$  have two more pole-free sectors than their  $\nu \in \mathbb{R} \setminus \mathbb{Z}$  counterparts: one contained in an upper or lower half-plane with  $u \sim \pm i$  and another contained in a lower or upper half-plane with  $u \sim \mp i$ .

Table 2: The pole-free sectors of MTW solutions  $u(z; \nu, \sigma)$  with  $0 < \sigma = \frac{n_1}{n_2} < 1$ , where the fraction  $\frac{n_1}{n_2}$  is expressed to lowest terms. The solution has  $n_2$  distinct branches and thus it suffices to consider the region  $-\pi/2 < \arg z \leq (2n_2 - \frac{1}{2})\pi$ .

$\nu$	$0 < \sigma = \frac{n_1}{n_2} < 1$	$z \rightarrow \infty$	Sector
$\nu \in \mathbb{R} \setminus \mathbb{Z}$	$n_1$ and $n_2$ have opposite parity	$u \sim 1$	$-\frac{\pi}{2} < \arg z < \frac{\pi}{2}$
	$n_1$ and $n_2$ are odd	$u \sim 1$ $u \sim -1$	$-\frac{\pi}{2} < \arg z < \frac{\pi}{2}$ $(n_2 - \frac{1}{2})\pi < \arg z < (n_2 + \frac{1}{2})\pi$
$\nu \in \mathbb{Z}$	$n_1$ and $n_2$ have opposite parity	$u \sim 1$	$-\frac{\pi}{2} < \arg z < \frac{\pi}{2}$
		$u \sim (-1)^{n_2+1}$	$(n_2 - \frac{1}{2})\pi < \arg z < (n_2 + \frac{1}{2})\pi$
	$n_1 \bmod 4 = 1$ and $n_2$ is odd	$u \sim 1$	$-\frac{\pi}{2} < \arg z < \frac{\pi}{2}$
		$u \sim (-1)^\nu i$	$\frac{n_2-1}{2}\pi < \arg z < \frac{n_2+1}{2}\pi$
		$u \sim -1$	$(n_2 - \frac{1}{2})\pi < \arg z < (n_2 + \frac{1}{2})\pi$
		$u \sim (-1)^{\nu+1} i$	$\frac{3n_2-1}{2}\pi < \arg z < \frac{3n_2+1}{2}\pi$
$n_1 \bmod 4 = 3$ and $n_2$ is odd	$u \sim 1$	$-\frac{\pi}{2} < \arg z < \frac{\pi}{2}$	
	$u \sim (-1)^{\nu+1} i$	$\frac{n_2-1}{2}\pi < \arg z < \frac{n_2+1}{2}\pi$	
	$u \sim -1$	$(n_2 - \frac{1}{2})\pi < \arg z < (n_2 + \frac{1}{2})\pi$	
	$u \sim (-1)^\nu i$	$\frac{3n_2-1}{2}\pi < \arg z < \frac{3n_2+1}{2}\pi$	

We identified tronquée solutions on sheets 1–4 by observing the movement and orientation of the pole fields as  $\sigma$  is varied between 0 and 1. As an example, Figure 12 shows the pole fields on the first sheet of the MTW solution with  $\nu = -1$  as  $\sigma$  increases through the critical value  $\sigma = 1/3$ . According to the fourth case in Table 2, we expect to find two pole-free sectors on the first sheet when  $\sigma = 1/3$ : within  $\pi < \arg z < 2\pi$ , on which  $u \sim -i$ ,  $z \rightarrow \infty$  and within  $5\pi/2 < \arg z < 7\pi/2$ , on which  $u \sim -1$ ,  $z \rightarrow \infty$ . As  $\sigma$  increases to  $1/3$  the pole fields in the upper-left quarter-plane and lower half-plane move towards  $z = \infty$ , as shown in the first two frames. When  $\sigma = 1/3$  the pole fields are out of the finite plane and as the pole fields return from  $z = \infty$  for  $\sigma > 1/3$  their orientations are changed (cf. the first and second rows). Note the similarities between Figures 12 and 8. In both figures poles and zeros move out of the finite plane, resulting in a pole-free region, and return differently aligned. In Figure 8 the poles and zeros move toward and return from  $\text{Re } \zeta = -\infty$  (or  $z = 0$ ) and in Figure 13 the poles and zeros move toward and return from  $\text{Re } \zeta = \infty$  (or  $z = \infty$ ).

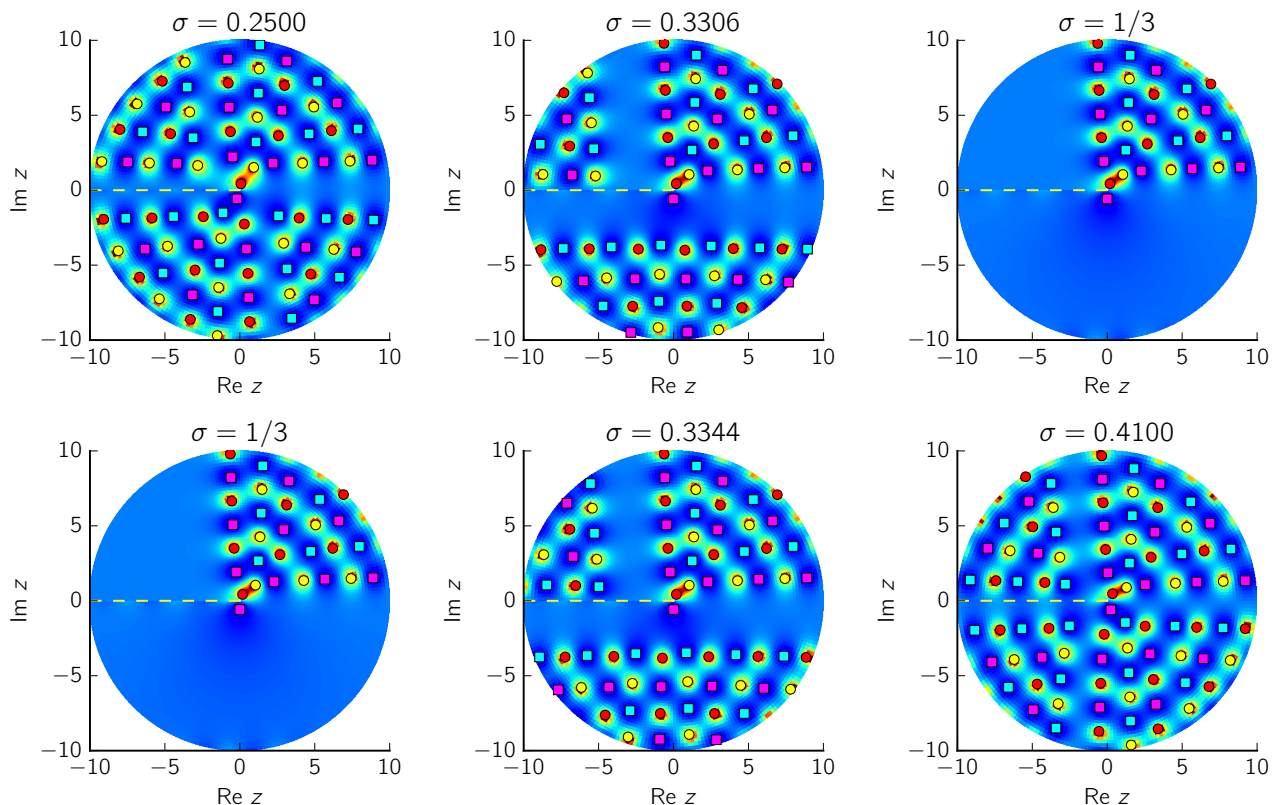


Figure 12: The pole fields move out of the finite plane and return with a different orientation as  $\sigma$  transitions through the critical value,  $\sigma = 1/3$  in this case. These pole fields are on the first sheet of the MTW solution with  $\nu = -1$ .

## 6.2 Analytical results for $0 < \sigma < 1$

To provide further justification for the empirical results in Table 2, we will make use of the following scaling Bäcklund transformation for  $P_{\text{III}}$ . Let  $u(z; \alpha, \beta, \gamma, \delta)$  denote a  $P_{\text{III}}$  solution and let  $c_1$  and  $c_2$  be constants, then the scaling transformation  $c_1^{-1}u(c_2z; \alpha, \beta, \gamma, \delta)$  maps  $u$  to another  $P_{\text{III}}$  solution with generally different parameter values [15]:

$$T_0(c_1, c_2) : u \mapsto u(z; \tilde{\alpha}, \tilde{\beta}, \tilde{\gamma}, \tilde{\delta}) := c_1^{-1}u(c_2z; \alpha, \beta, \gamma, \delta), \quad (43)$$

$$\tilde{\alpha} = c_1c_2\alpha, \quad \tilde{\beta} = c_1^{-1}c_2\beta, \quad \tilde{\gamma} = c_1^2c_2^2\gamma, \quad \tilde{\delta} = c_1^{-2}c_2^2\delta. \quad (44)$$

We require that the parameters be real MTW parameters (1), i.e.,

$$\alpha = -\beta = 2\nu, \quad \nu \in \mathbb{R}, \quad \tilde{\alpha} = -\tilde{\beta} = 2\tilde{\nu}, \quad \tilde{\nu} \in \mathbb{R}, \quad \gamma = \tilde{\gamma} = 1 = -\tilde{\delta} = -\delta. \quad (45)$$

From (44) and (45) we deduce that  $c_1^4 = c_2^4 = 1$  and that  $c_1$  and  $c_2$  must either both be real or both be imaginary. In addition, if  $c_1$  and  $c_2$  are both imaginary, then we require  $\alpha = \beta = 0$  for  $\tilde{\alpha} = -\tilde{\beta}$  to be satisfied. Thus, we only consider the following special cases of  $T_0(c_1, c_2)$  applied to solutions with MTW parameters:

$$T_0((-1)^m, e^{-i\pi m}) : \quad u(z; 2\nu, -2\nu, 1, -1) = (-1)^m u(e^{-i\pi m} z; 2\nu, -2\nu, 1, -1), \quad (46)$$

$$T_0((-1)^{m+1}, e^{-i\pi m}) : \quad u(z; -2\nu, 2\nu, 1, -1) = (-1)^{m+1} u(e^{-i\pi m} z; 2\nu, -2\nu, 1, -1), \quad (47)$$

$$T_0(-i, ie^{-i\pi m}) : \quad u(z; 0, 0, 1, -1) = iu(ie^{-i\pi m} z; 0, 0, 1, -1), \quad (48)$$

$$T_0(i, ie^{-i\pi m}) : \quad u(z; 0, 0, 1, -1) = -iu(ie^{-i\pi m} z; 0, 0, 1, -1). \quad (49)$$

Since we are interested in solutions on the  $s$ -th sheets with  $s > 0$  we let  $m$  be an integer with  $m \geq 2$ . Note that the transformation in (47) changes the signs of the first two parameters whereas (46), (48) and (49) are auto-Bäcklund transformations, i.e., transformations that preserve parameter values. The following results will be used to account for the observations in Table 2.

**Lemma 1.** *Let  $T_0(c_1, e^{-i\theta})$  denote any of the transformations (46)–(49). The MTW solutions with  $\nu \in \mathbb{R}$  and  $0 < \sigma < 1$ ,  $\sigma \neq \sigma_c$  (see (13) and (14)) are closed under  $T_0(c_1, e^{-i\theta})$ , i.e.,*

$$u(z; \tilde{\nu}, \sigma) = T_0(c_1, e^{-i\theta})u(z; \nu, \sigma) = c_1^{-1}u(e^{-i\theta}z; \nu, \sigma), \quad (50)$$

only if

$$B(\sigma, \tilde{\nu}) = c_1^{-1}e^{-i\theta\sigma}B(\sigma, \nu), \quad (51)$$

where  $B(\sigma, \nu)$  is defined in (12). If  $T_0(c_1, e^{-i\theta})$  denotes the transformation (46), then  $\tilde{\nu} = \nu$ ; if  $T_0(c_1, e^{-i\theta})$  is (47), then  $\tilde{\nu} = -\nu$  and if  $T_0(c_1, e^{-i\theta})$  is (48) or (49), then  $\tilde{\nu} = \nu = 0$ .

*Proof.* As stated in section 2.2.1, a generic  $P_{\text{III}}$  solution with MTW parameters (1) has a unique small- $z$  expansion (8) for fixed  $B$ ,  $\nu$  and  $\sigma$ . What characterizes an MTW  $P_{\text{III}}$  solution for fixed  $\nu$  and  $\sigma \neq \sigma_c$ , however, is the coefficient of the leading order term of the unique small- $z$  expansion (8):  $B = B(\sigma, \nu)$ , defined in (12). Thus, to prove (50), it suffices to show that the coefficients of the leading order terms on the left and right-hand sides of (50) match, which is the condition expressed in (51).  $\square$

**Theorem 1.** *The MTW solutions with  $\nu \in \mathbb{R}$  and  $0 < \sigma < 1$ ,  $\sigma \neq \sigma_c$  are closed under the transformations (46)–(49) with  $m \geq 2$  only if, respectively,*

$$\nu \in \mathbb{R} \quad \text{and} \quad \sigma = \begin{cases} \frac{2n+1}{2k-1} & \text{with } m = 2k - 1, \text{ or} \\ \frac{n}{k} & \text{with } m = 2k, \end{cases} \quad (52)$$

$$\nu \in \mathbb{Z} \quad \text{and} \quad \sigma = \begin{cases} \frac{2n+1}{2k-2} & \text{with } m = 2k - 2, \text{ or} \\ \frac{2n}{2k-1} & \text{with } m = 2k - 1, \end{cases} \quad (53)$$

$$\nu = 0 \quad \text{and} \quad \sigma = \frac{4n+1}{2k-1} \quad \text{with } m = k \quad \text{and} \quad (54)$$

$$\nu = 0 \quad \text{and} \quad \sigma = \frac{4n+3}{2k-1} \quad \text{with } m = k, \quad (55)$$

where  $n$  and  $k$  are integers such that  $k \geq 2$  and  $0 < \sigma < 1$ .

*Proof.* According to Lemma 1 the MTW solutions are closed under the transformations (46)–(49) only if (51) is satisfied. For (46),  $c_1 = (-1)^m$ ,  $c_2 = e^{-i\theta} = e^{-i\pi m}$ ,  $\tilde{\nu} = \nu$  and thus (51) reduces to

$$e^{i\pi m\sigma} = (-1)^m.$$

This equation is satisfied only if  $m\sigma\pi = n_1\pi$ , i.e.,  $\sigma = n_1/m$ , where  $n_1$  and  $m$  are integers with the same parity such that  $0 < \sigma < 1$ . If  $m$  is even, say  $m = 2k$ , then  $\sigma = \frac{n}{k}$  and if  $m$  is odd with  $m = 2k - 1$ , then  $\sigma = \frac{2n+1}{2k-1}$  where  $n$  and  $k$  are integers such that  $k \geq 2$  and  $0 < \sigma < 1$ .

For the transformation (47),  $\tilde{\nu} = -\nu$ ,  $c_1 = (-1)^{m+1}$  and  $c_2 = e^{-i\pi m}$ . Thus, (51) implies that we require  $B(\sigma, -\nu) = \pm B(\sigma, \nu)$  since  $B(\sigma, \nu) \in \mathbb{R}$  for  $\sigma, \nu \in \mathbb{R}$ . According to Lemma 2 in the Appendix,  $B(\sigma, -\nu) = B(\sigma, \nu)$  only if  $\nu \in \mathbb{Z}$  and  $B(\sigma, -\nu) = -B(\sigma, \nu)$  only if  $\nu = n + \frac{1}{2}$ ,  $n \in \mathbb{Z}$ . However, we need only consider  $\nu \in \mathbb{Z}$  since MTW solutions do not exist when  $\nu = -n - \frac{1}{2}$ ,  $n \geq 0$ .<sup>7</sup> Hence, if  $\nu \in \mathbb{Z}$ , then (51) becomes

$$e^{i\pi m\sigma} = (-1)^{m+1}. \quad (56)$$

This equation is satisfied only if  $m\sigma\pi = n_1\pi$ , or,  $\sigma = n_1/m$  where  $n_1$  and  $m$  are integers with opposite parity such that  $0 < \sigma < 1$ . If  $m$  is even this reduces to  $\sigma = \frac{2n+1}{2k-2}$  and if  $m$  is odd this reduces to  $\sigma = \frac{2n}{2k-1}$  where  $n$  and  $k$  are integers such that  $k \geq 2$  and  $0 < \sigma < 1$ .

For the transformations (48) and (49), respectively,  $c_1 = \mp i$ ,  $c_2 = ie^{-i\pi m}$  and  $\tilde{\nu} = \nu = 0$ . Thus, (51) becomes

$$e^{i\pi(m-\frac{1}{2})\sigma} = \pm i.$$

For the transformation (48), the equation is satisfied only if  $(m - \frac{1}{2})\sigma\pi = (n_1 - \frac{1}{2})\pi$  with  $n_1$  odd, i.e., only if  $\sigma = (2n_1 - 1)/(2m - 1)$ , which is equivalent to (54). Similarly, for (49) the equation is satisfied only if  $\sigma = (2n_1 - 1)/(2m - 1)$ , with  $n_1$  even, which is equivalent to (55).  $\square$

**Corollary 1.** *If  $0 < \sigma = \frac{n_1}{n_2} < 1$ ,  $\sigma \neq \sigma_c$ , where  $n_1$  and  $n_2$  are positive integers and  $\frac{n_1}{n_2}$  is expressed to lowest terms, then the MTW solution  $u(z; \nu, \sigma)$  is an algebraically branched solution with  $n_2$  distinct branches.*

*Proof.* This follows from (52): setting  $m = 2n_2$  in (46) we have

$$u(z; \nu, \sigma) = T_0(1, e^{-2i\pi n_2})u(z; \nu, \sigma) = u(e^{-2i\pi n_2}z; \nu, \sigma), \quad \sigma = \frac{n_1}{n_2}. \quad (57)$$

Since  $\sigma = \frac{n_1}{n_2}$  is expressed to lowest terms,  $n_2$  is the smallest positive integer for which (57) holds and thus the solution has exactly  $n_2$  distinct branches.  $\square$

To generate the results in Table 2 we shall use repeated applications of the transformations (46)–(49).

**Corollary 2.** *For the transformations and values of  $\nu$  and  $\sigma$  specified in Theorem 1, the MTW solution  $u(z; \nu, \sigma)$  is also closed under  $T_0^n(c_1, e^{-i\theta})$ ,  $n \geq 1$  and*

$$T_0^n(c_1, e^{-i\theta})u(z; \nu, \sigma) = T_0(c_1^n, e^{-in\theta})u(z; \nu, \sigma) = c_1^{-n}u(e^{-in\theta}z; \nu, \sigma) = u(z; \hat{\nu}, \sigma), \quad (58)$$

where  $\hat{\nu} = \nu$  if  $T_0(c_1, e^{-i\theta})$  is one of the auto-Bäcklund transformations (46), (48) or (49) and  $\hat{\nu} = (-1)^n\nu$  if  $T_0(c_1, e^{-i\theta})$  is the transformation (47) that reflects the parameter  $\nu$ .

---

<sup>7</sup>If  $\nu = -n - \frac{1}{2}$ ,  $n \geq 0$ , then one set of limiting MTW solutions is the left-end MTW solutions, discussed in section 5.1. As pointed out in the final paragraph of that section and in Theorem 3 in the Appendix, the transformation (47) with  $m = 0$ ,  $u(z; -\nu, \sigma) = -u(z; \nu, \sigma)$ , gives the relationship between the left-end MTW solutions and the MTW solutions.

*Proof.* If  $u(z; \nu, \sigma)$  is closed under  $T_0(c_1, e^{-i\theta})$ , then

$$u(z; \tilde{\nu}, \sigma) = T_0(c_1, e^{-i\theta})u(z; \nu, \sigma) = c_1^{-1}u(e^{-i\theta}z; \nu, \sigma). \quad (59)$$

If  $T_0(c_1, e^{-i\theta})$  denotes (46), (48) or (49), then  $\tilde{\nu} = \nu$  and thus it follows from Theorem 1 that  $u(z; \tilde{\nu}, \sigma)$  is also closed under  $T_0(c_1, e^{-i\theta})$ . If  $T_0(c_1, e^{-i\theta})$  denotes (47), then  $\tilde{\nu} = -\nu$  and since  $\nu \in \mathbb{Z}$ ,  $\tilde{\nu} \in \mathbb{Z}$  and thus it follows from Theorem 1 that  $u(z; \tilde{\nu}, \sigma)$  is also closed under  $T_0(c_1, e^{-i\theta})$ . Hence, from (59) we have

$$\begin{aligned} u(z; \hat{\nu}, \sigma) &= T_0(c_1, e^{-i\theta})u(z; \tilde{\nu}, \sigma) = T_0^2(c_1, e^{-i\theta})u(z; \nu, \sigma) \\ &= T_0(c_1, e^{-i\theta})c_1^{-1}u(e^{-i\theta}z; \nu, \sigma) = c_1^{-2}u(e^{-2i\theta}z; \nu, \sigma) = T_0(c_1^2, e^{-2i\theta})u(z; \nu, \sigma), \end{aligned}$$

where  $\hat{\nu} = \tilde{\nu} = \nu$  if  $T_0(c_1, e^{-i\theta})$  is (46), (48) or (49) and  $\hat{\nu} = -\tilde{\nu} = -(-\nu) = (-1)^2\nu$  if  $T_0(c_1, e^{-i\theta})$  is (47). Repeating this argument  $n - 1$  times, we arrive at the result (58).  $\square$

In addition to the scaling transformations (46)–(49), we require the Bäcklund transformation  $T_\varepsilon$ , defined by (38), to account for the results in Table 2.

**Theorem 2.** *For  $\nu \in \mathbb{R}$  and  $0 < \sigma < 1$ ,  $\sigma \neq \sigma_c$ , the MTW solutions are closed under  $T_\varepsilon$ , i.e.,*

$$u(z; \nu + \varepsilon, \sigma) = T_\varepsilon u(z; \nu, \sigma), \quad \varepsilon^2 = 1, \quad \nu \neq \frac{1}{2\varepsilon}(\sigma - 1). \quad (60)$$

*Proof.* From the definition of the Bäcklund transformation  $T_\varepsilon$  in (38), the right-hand side of (60) is a solution of P<sub>III</sub> with MTW parameter  $\nu + \varepsilon$  and therefore, as stated in section 2.2.1, it has a unique small- $z$  expansion of the form (8). To show that this solution is an MTW solution with parameter  $\nu + \varepsilon$  and thereby prove the result (60), it is sufficient to show, by the same argument given in the proof of Lemma 1, that the coefficients of the leading order terms of the small- $z$  expansions on the left and right-hand sides of (60) match. Substituting the small- $z$  expansion (8)–(12) into  $T_\varepsilon$ , we find that the coefficient of the leading order term is

$$\left( \frac{2\varepsilon\nu + 1 + \sigma}{2\varepsilon\nu + 1 - \sigma} \right) B(\sigma, \nu). \quad (61)$$

The leading order coefficient on the left-hand side of (60) is  $B(\sigma, \nu + \varepsilon)$  and using (12) and the property  $\Gamma(z) = (z - 1)\Gamma(z - 1)$ , it follows that

$$B(\sigma, \nu + \varepsilon) = \left( \frac{2\varepsilon\nu + 1 + \sigma}{2\varepsilon\nu + 1 - \sigma} \right) B(\sigma, \nu), \quad (62)$$

and thus (61) and (62) match.  $\square$

It follows from Theorem 2 that  $u(z; \nu + k, \sigma) = T_1^k u(z; \nu, \sigma)$  and  $u(z; \nu - k, \sigma) = T_{-1}^k u(z; \nu, \sigma)$  for  $\sigma \neq \sigma_c$  and  $k \geq 1$ , and thus it suffices to apply  $T_1$  only to solutions with  $\nu \geq 0$  and  $T_{-1}$  only to solutions with  $\nu \leq 0$ . Hence, the cases implied by the restriction on  $\nu$  in (60), which follow from the denominator in (61)–(62), need not arise.

The final results required to generate the empirical results in Table 2 using Bäcklund transformations are the large- $z$  behaviors in certain sectors of the solutions  $T_0^n(c_1, e^{-i\theta})u(z; \nu, \sigma)$  and the solutions obtained from compositions of  $T_\varepsilon^k$  with  $T_0^n(c_1, e^{-i\theta})u(z; \nu, \sigma)$ .

**Proposition 1.** *For the transformations and values of  $\nu$  and  $\sigma$  specified in Theorem 1,*

$$u(z; \hat{\nu}, \sigma) = T_0^n(c_1, e^{-i\theta})u(z; \nu, \sigma) = T_0(c_1^n, e^{-in\theta})u(z; \nu, \sigma) = c_1^{-n}u(e^{-in\theta}z; \nu, \sigma) \sim c_1^{-n}, \quad (63)$$

and

$$u(z; \widehat{\nu} + k\varepsilon, \sigma) = T_\varepsilon^k u(z; \widehat{\nu}, \sigma) = T_\varepsilon^k \circ T_0^n(c_1, e^{-i\theta}) u(z; \nu, \sigma) \sim \begin{cases} c_1^{-n}, & \text{if } c_1^{-2n} = 1, \\ (-1)^k c_1^{-n}, & \text{if } c_1^{-2n} = -1, \end{cases} \quad (64)$$

where (63) and (64) are valid for

$$z \rightarrow \infty, \quad -\frac{\pi}{2} + n\theta < \arg z < \frac{\pi}{2} + n\theta, \quad (65)$$

and  $\varepsilon^2 = 1$ ,  $\widehat{\nu} = \nu$  if  $T_0(c_1, e^{-i\theta})$  is (46), (48) or (49) and  $\widehat{\nu} = (-1)^n \nu$  if  $T_0(c_1, e^{-i\theta})$  is (47).

*Proof.* The result (63) follows from Corollary 2 and the large- $z$  formula (5):

$$\begin{aligned} u(z; \widehat{\nu}, \sigma) = T_0^n(c_1, e^{-i\theta}) u(z; \nu, \sigma) &= c_1^{-n} u(e^{-in\theta} z; \nu, \sigma) \\ &\sim c_1^{-n} + \mathcal{O}\left((e^{-in\theta} z)^{-\nu-1/2} \exp[-2e^{-in\theta} z]\right), \end{aligned} \quad (66)$$

for  $z \rightarrow \infty$ ,  $-\frac{\pi}{2} + n\theta < \arg z < \frac{\pi}{2} + n\theta$ .

It follows from Theorem 2 that the large- $z$  behavior of  $u(z; \widehat{\nu} + \varepsilon, \sigma)$  on (65) can be obtained by substituting (66) into (38) and letting  $z \rightarrow \infty$ , in which case we find

$$u(z; \widehat{\nu} + \varepsilon, \sigma) = T_\varepsilon u(z; \widehat{\nu}, \sigma) = T_\varepsilon \circ T_0^n(c_1, e^{-i\theta}) u(z; \nu, \sigma) \sim -c_1^{-n} \frac{\varepsilon(c_1^{-2n} - 1)z + (2\varepsilon\widehat{\nu} + 1)c_1^{-n}}{\varepsilon(c_1^{-2n} - 1)z - (2\varepsilon\widehat{\nu} + 1)c_1^{-n}}, \quad (67)$$

with the same exponential-order correction term as in (66). For the transformations (46)–(49),  $c_1^{-2n} = 1$  or  $c_1^{-2n} = -1$ , hence

$$u(z; \widehat{\nu} + \varepsilon, \sigma) = T_\varepsilon u(z; \widehat{\nu}, \sigma) \sim \begin{cases} c_1^{-n} + \mathcal{O}\left((e^{-i\theta} z)^{-\nu-1/2} \exp[-2e^{-i\theta} z]\right), & \text{if } c_1^{-2n} = 1, \\ -c_1^{-n} + \mathcal{O}\left((e^{-i\theta} z)^{-\nu-1/2} \exp[-2e^{-i\theta} z]\right), & \text{if } c_1^{-2n} = -1, \end{cases} \quad (68)$$

for  $z \rightarrow \infty$ ,  $-\pi/2 + n\theta < \arg z < \pi/2 + n\theta$ , provided  $\widehat{\nu} \neq -\frac{1}{2}$  if  $\varepsilon = 1$  and  $c_1^{-2n} = 1$  and  $\widehat{\nu} \neq \frac{1}{2}$  if  $\varepsilon = -1$  and  $c_1^{-2n} = 1$ . However, as noted in the paragraph below the proof of Theorem 2, these cases need not be considered. Hence, the leading order large- $z$  behaviors of  $u(z; \widehat{\nu} + \varepsilon, \sigma)$  and  $u(z; \widehat{\nu}, \sigma)$  are the same on  $-\pi/2 + n\theta < \arg z < \pi/2 + n\theta$  if  $c_1^{-2n} = 1$  (cf. (68) and (66)) but if  $c_1^{-2n} = -1$ , then the leading order behaviors differ in sign. Note that in both cases,  $c_1^{-2n} = 1$  and  $c_1^{-2n} = -1$ , the correction terms are of the same order in (68) and (66). Thus, if we apply  $T_\varepsilon$  to  $u(z; \widehat{\nu} + \varepsilon, \sigma)$  on  $-\pi/2 + n\theta < \arg z < \pi/2 + n\theta$ , let  $z \rightarrow \infty$  and use (68), then we again arrive at (67), with the same correction term as in (66), except that  $\widehat{\nu}$  is replaced by  $\widehat{\nu} + \varepsilon$  in (67) and  $c_1^{-n}$  is replaced by  $-c_1^{-n}$  if  $c_1^{-2n} = -1$  in (68). We conclude, as before, that the leading order large- $z$  behaviors of  $u(z; \widehat{\nu} + 2\varepsilon, \sigma)$  and  $u(z; \widehat{\nu} + \varepsilon, \sigma)$  are the same on  $-\pi/2 + n\theta < \arg z < \pi/2 + n\theta$  if  $c_1^{-2n} = 1$  but if  $c_1^{-2n} = -1$ , then the leading order behaviors differ in sign. Repeating this argument another  $k - 2$  times we arrive at the result (64).  $\square$

**Proposition 2.** *The empirical results in Table 2 follow from the preceding analytical results: Theorem 1, Corollaries 1 and 2 and Proposition 1.*

*Proof.* Consider the first case in Table 2:  $\nu \in \mathbb{R} \setminus \mathbb{Z}$  and  $0 < \sigma = \frac{n_1}{n_2} < 1$ , where the fraction  $\frac{n_1}{n_2}$  is expressed to lowest terms and  $n_1$  and  $n_2$  have opposite parity. According to Theorem 1, of the transformations (46)–(49),  $u(z; \nu, \sigma)$  is closed under (46) only, with  $m = 2n_2$ . As shown in the proof of Corollary 1, this transformation maps the solution from sheet  $s$  to sheet  $s + n_2$ . However, according to Corollary 1, the solution has  $n_2$  distinct branches. Thus, henceforth we need not consider the transformation (46) with  $m = 2n_2$  and we may restrict our attention

to sheets 0 to  $n_2 - 1$ , or the region  $-\frac{\pi}{2} < \arg z < (2n_2 - \frac{1}{2})\pi$ . We conclude that the only inference that can be made regarding  $u(z; \nu, \sigma)$  based on the transformations (46)–(49) is that it has  $n_2$  distinct branches. As with all MTW solutions,  $u(z; \nu, \sigma)$  has a pole-free sector within  $-\pi/2 < \arg z < \pi/2$  on which  $u \sim 1$  (see the large- $z$  formula (5)). These conclusions are consistent with the results for the first case in Table 2.

Now let  $\nu \in \mathbb{R} \setminus \mathbb{Z}$  and suppose  $n_1$  and  $n_2$  are both odd (the second case in Table 2). Then, of the transformations (46)–(49),  $u(z; \nu, \sigma)$  is closed under (46) only, with  $m = n_2$  (and  $m = 2n_2$  which, as mentioned above, need not be considered). Thus, we set  $c_1 = -1$ ,  $c_2 = e^{-i\theta} = e^{-i\pi n_2}$ ,  $\hat{\nu} = \nu$  and, since we require  $-\frac{\pi}{2} < \arg z < (2n_2 - \frac{1}{2})\pi$ ,  $n = 1$  in (63) and (65) and obtain

$$u(z; \nu, \sigma) \sim -1, \quad z \rightarrow \infty, \quad (n_2 - \frac{1}{2})\pi < \arg z < (n_2 + \frac{1}{2})\pi,$$

which is in agreement with the second case in Table 2.

Let  $\nu \in \mathbb{Z}$  and suppose  $n_1$  and  $n_2$  have opposite parity. Of the transformations (46)–(49),  $u(z; \nu, \sigma)$  is closed under (47) only with  $m = n_2$ . Thus,  $c_1 = (-1)^{n_2+1}$ ,  $c_2 = e^{-i\theta} = e^{-i\pi n_2}$ ,  $\hat{\nu} = -\nu$  and  $n = 1$  in (63) and (65):

$$u(z; -\nu, \sigma) \sim (-1)^{n_2+1}, \quad z \rightarrow \infty, \quad (n_2 - \frac{1}{2})\pi < \arg z < (n_2 + \frac{1}{2})\pi,$$

which agrees with the third case in Table 2.

Now consider the final two cases in Table 2:  $\nu \in \mathbb{Z}$  and  $n_1$  and  $n_2$  are odd. Of the transformations (46)–(49),  $u(z; \nu, \sigma)$  is closed under (46) and, if  $\nu = 0$ , (48) (if  $n_1 \bmod 4 = 1$ ) or (49) (if  $n_1 \bmod 4 = 3$ ). For solutions with  $\nu \in \mathbb{Z} \setminus \{0\}$ , we also consider compositions of  $T_\varepsilon^k$  with (48) (if  $n_1 \bmod 4 = 1$ ) or (49) (if  $n_1 \bmod 4 = 3$ ) applied to  $u(z; \nu, \sigma)$  with  $\nu = 0$ . For the transformations (48) and (49), respectively,  $m = (n_2 + 1)/2$ ,  $c_1 = \mp i$ ,  $c_2 = e^{-i\theta} = ie^{-i\pi m} = e^{-i\pi n_2/2}$ ,  $\hat{\nu} = \nu = 0$  and  $n = 1, 2, 3$  in (64) and (65):

$$u(z; k\varepsilon, \sigma) = T_\varepsilon^k \circ T_0^n(\mp i, e^{-i\pi n_2/2})u(z; 0, \sigma) \sim \begin{cases} -1 & \text{even } n \\ (-1)^k(\pm i)^n & \text{odd } n \end{cases}, \quad (69)$$

$$z \rightarrow \infty, \quad (nn_2 - 1)\frac{\pi}{2} < \arg z < (nn_2 + 1)\frac{\pi}{2}, \quad n = 1, 2, 3, \quad k \geq 0, \quad (70)$$

which is equivalent to the results for the fifth and sixth cases in Table 2. For the transformation (46),  $m = n_2$ ,  $c_1 = -1$ ,  $c_2 = e^{-i\theta} = e^{-i\pi n_2}$  and  $n = 1$  in (63) and (65):

$$u(z; \nu, \sigma) \sim -1, \quad z \rightarrow \infty, \quad (n_2 - \frac{1}{2})\pi < \arg z < (n_2 + \frac{1}{2})\pi, \quad \nu \in \mathbb{Z}. \quad (71)$$

However, (71) is the same as (69) and (70) with  $n = 2$ . The latter observation also follows from the fact that the transformation (46) is the same as two applications of (48) or (49) for the cases under consideration (the final two cases in Table 2):  $T_0^2(\mp i, e^{-i\pi n_2/2}) = T_0((\mp i)^2, (e^{-i\pi n_2/2})^2) = T_0(-1, e^{-i\pi n_2})$ , see (58).  $\square$

### 6.3 Examples for $0 < \sigma < 1$

Figure 13 illustrates solutions described by the third case in Table 2:  $\nu \in \mathbb{Z}$  and  $\sigma = \frac{n_1}{n_2} = \frac{1}{2}$ . According to Corollary 1 the solutions in Figure 13 have two distinct branches, as can be confirmed by considering the colors above and below the branch cuts in the second row of the figure. As shown in the proof of Proposition 2, the pole-free sectors of solutions corresponding to the third case in Table 2 follow from the transformation (47). This transformation is unique among the scaling transformations (46)–(49) in that it gives the relationship between different regions of different solutions, whereas (46), (48) and (49) describe relationships between

different regions of the same solution. Specifically, according to Theorem 1, the relationship between the two solutions in Figure 13 is given by

$$u\left(z; -1, \frac{1}{2}\right) = T_0(-1, e^{-2i\pi})u\left(z; 1, \frac{1}{2}\right) = -u\left(e^{-2i\pi}z; 1, \frac{1}{2}\right). \quad (72)$$

Thus, the 0th and 1st sheets of the  $\nu = -1$  solution are the negatives of the 1st and 0th sheets, respectively, of the  $\nu = 1$  solution.

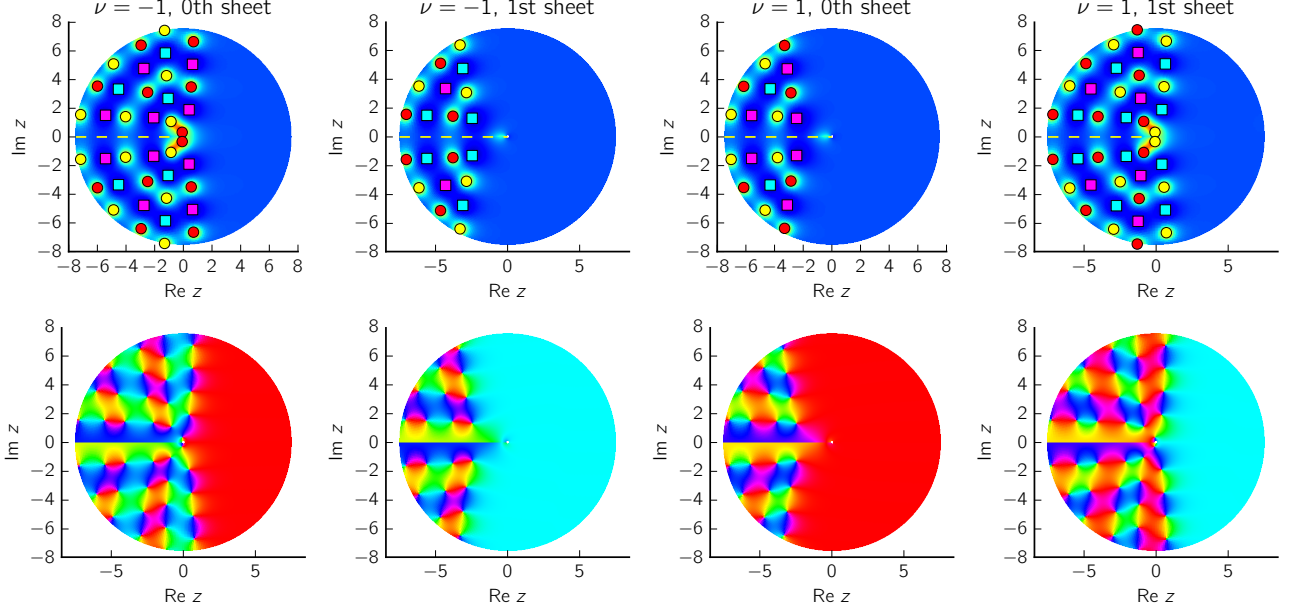


Figure 13: Two doubly branched MTW solutions ( $\sigma = \frac{1}{2}$ ) that are related according to (72).

Figure 14 illustrates solutions corresponding to the fourth case in Table 2:  $\nu \in \mathbb{Z}$  and  $\sigma = \frac{1}{7} = \frac{n_1}{n_2}$ . Since the solutions are displayed within  $-\pi \leq \arg z \leq 9\pi$  (and the corresponding region in the  $\zeta$ -plane,  $-2\pi \leq \text{Im } \zeta \leq 18\pi$ ), three of the four pole-free regions in Table 2 are visible: within  $-\pi/2 < \arg z < \pi/2$ ,  $3\pi < \arg z < 4\pi$  and  $13\pi/2 < \arg z < 14\pi/2$  on which  $u \sim 1$ ,  $u \sim (-1)^\nu i$  and  $u \sim -1$ , respectively, for  $z \rightarrow \infty$ . According to Theorem 1, the solution with  $\nu = 0$  in the first two columns of Figure 14 is closed under  $T_0^n(-i, e^{-7i\pi/2})$  and  $T_0^n(-1, e^{-7i\pi})$ ,  $n \geq 2$ . However, since  $T_0^2(-i, e^{-7i\pi/2}) = T_0(-1, e^{-7i\pi})$ , see (58), we need only consider  $T_0^n(-i, e^{-7i\pi/2})$ . Thus,

$$u(z; 0, \sigma) = T_0^n(-i, e^{-7i\pi/2})u(z; 0, \sigma) = i^n u(e^{-7i\pi n/2}z; 0, \sigma), \quad \sigma = \frac{1}{7}. \quad (73)$$

Unlike the  $\nu = 0$  solution, the solutions in the third through fifth columns of Figure 14 are not closed under  $T_0(-i, e^{-7i\pi/2})$  (this follows from Theorem 1):

$$u(z; -k, \sigma) \neq T_0(-i, e^{-7i\pi/2})u(z; -k, \sigma) = iu(e^{-7i\pi/2}z; -k, \sigma), \quad k = 1, 2, \quad \sigma = \frac{1}{7}. \quad (74)$$

However, according to Theorems 1 and 2 the following transformations are applicable to the  $\nu \neq 0$  solutions in Figure 14:

$$u(z; -k, \sigma) = T_0(-1, e^{-7i\pi})u(z; -k, \sigma) = -u(e^{-7i\pi}z; -k, \sigma), \quad k = 1, 2, \quad \sigma = \frac{1}{7}, \quad (75)$$

and

$$u(z; -k, \sigma) = T_{-1}^k u(z; 0, \sigma), \quad k = 1, 2. \quad (76)$$

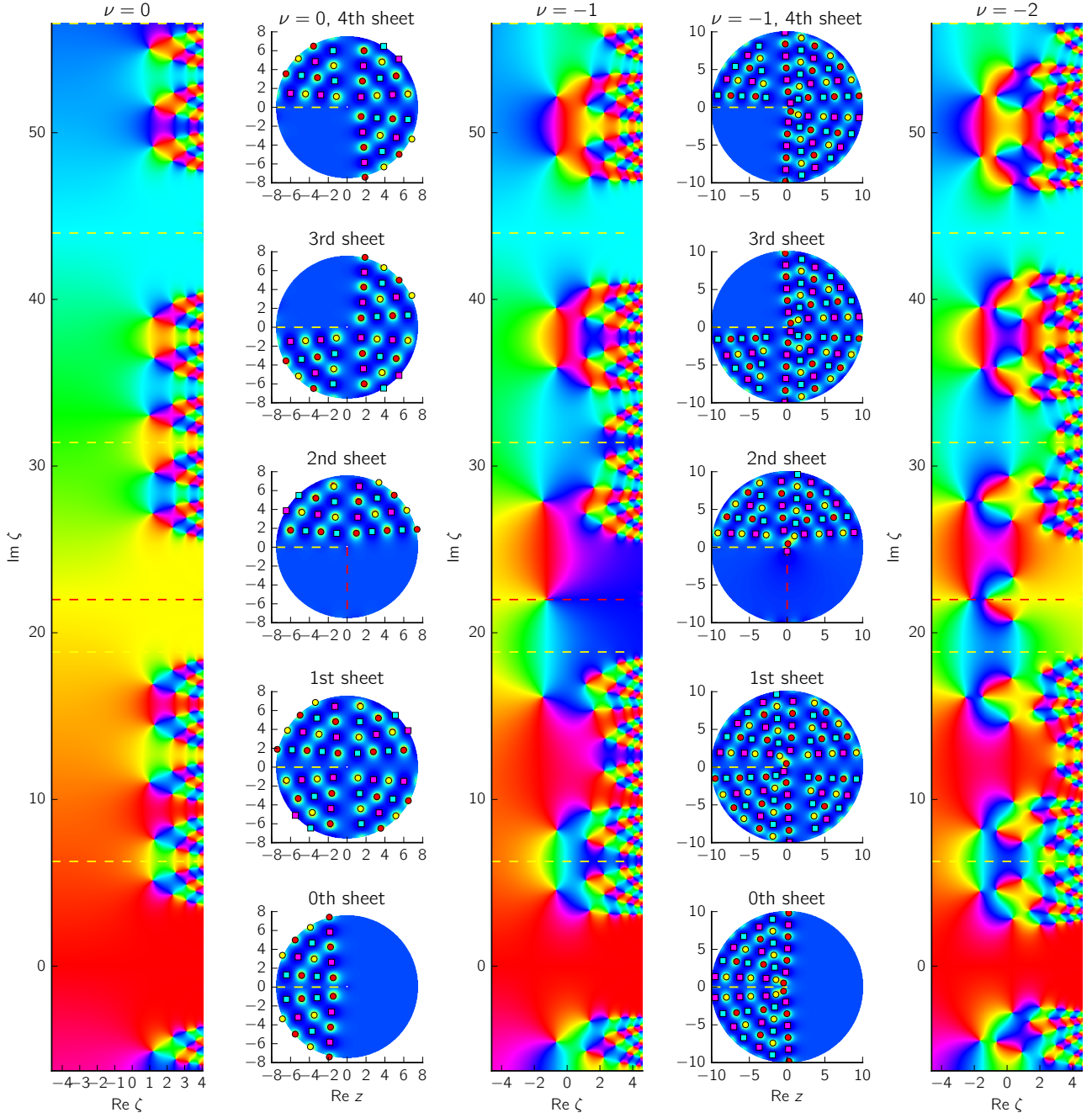


Figure 14: MTW solutions with  $\nu \in \mathbb{Z}$  and  $\sigma = \frac{1}{7}$ , corresponding to the fourth case in Table 2, on sheets 0 to 4. The second and fourth columns are pole field plots, while the first, third and fifth columns are phase portraits of the solutions that indicate the solution values on the pole-free sectors according to the color wheel at the top of Figure 10. The solutions exhibit certain symmetries and asymmetries in accordance with (73)–(76). Relationships between (i) the poles and zeros of the same solution and (ii) the poles and zeros of the different solutions are described by (77) and (78)–(79), respectively.

It was shown in Proposition 2 that the pole-free sectors of the solutions in Figure 14 follow from the transformations in (73), (75) and (76). Now we also consider the action of these transformations upon the simple poles and zeros of the MTW solutions in the  $z$ -plane (see Table 1). Suppose  $u(z; \nu, \sigma) \sim \pm 1/(z - z_0)$  or  $u(z; \nu, \sigma) \sim \pm(z - z_0)$ ,  $z \rightarrow z_0$ ,  $z_0 \neq 0$ , then if the MTW solutions are closed under  $T_0(c_1, e^{-i\theta})$  it follows from (50) that, respectively,

$$u(z; \tilde{\nu}, \sigma) \sim \frac{\pm c_1^{-1} e^{i\theta}}{z - e^{i\theta} z_0} \quad \text{and} \quad u(z; \tilde{\nu}, \sigma) \sim \pm c_1^{-1} e^{-i\theta} (z - e^{i\theta} z_0), \quad z \rightarrow e^{i\theta} z_0. \quad (77)$$

Each of the solutions in Figure 14 is closed under  $T_0(-1, e^{-7i\pi})$ , see (73) with  $n = 2$  and (75). Thus we see in all the columns of Figure 14 that  $T_0(-1, e^{-7\pi i})$  transforms poles with residue  $\pm 1$  and zeros with  $u' = \pm 1$  at  $z_0$  to poles and zeros of the same solution at  $e^{i\theta} z_0 = e^{7\pi i} z_0$  with residue  $\pm c_1^{-1} e^{i\theta} = \pm 1$  and  $u' = \pm c_1^{-1} e^{-i\theta} = \pm 1$ , respectively. For the solution in the first two columns we see that  $T_0(-i, e^{-7i\pi/2})$  rotates poles and zeros through  $\arg e^{i\theta} = \frac{7}{2}\pi$ ; the residues of the rotated poles are **preserved** since  $\pm c_1^{-1} e^{i\theta} = \pm 1$  while the derivative values of the rotated zeros are **reversed** since  $\pm c_1^{-1} e^{-i\theta} = \mp 1$ .

To consider the action of  $T_\varepsilon$  upon the poles and zeros of the MTW solutions, we substitute the two leading order terms of the Laurent expansion about a pole,

$$u(z; \nu, \sigma) = \frac{c}{z - z_0} - \frac{2\nu + c}{2z_0} + \mathcal{O}((z - z_0)), \quad z \rightarrow z_0, \quad z_0 \neq 0, \quad c^2 = 1,$$

and the Taylor expansion about a zero,

$$u(z; \nu, \sigma) = c(z - z_0) + \frac{2\nu + c}{2z_0}(z - z_0)^2 + \mathcal{O}((z - z_0)^3), \quad z \rightarrow z_0, \quad z_0 \neq 0 \quad c^2 = 1,$$

into (38). The poles are transformed to

$$u(z; \nu + \varepsilon) = T_\varepsilon u(z; \nu, \sigma) = \begin{cases} -\frac{\nu^2 + 3\varepsilon\nu + \frac{5}{4} + z_0^2}{z_0(4\nu + 2\varepsilon)} + \mathcal{O}((z - z_0)), & \text{if } c = \varepsilon, \\ \frac{\varepsilon}{z - z_0} - \frac{2(\nu + \varepsilon) + \varepsilon}{2z_0} + \mathcal{O}((z - z_0)) & \text{if } c = -\varepsilon, \end{cases}, \quad \varepsilon^2 = 1, \quad (78)$$

and the zeros are transformed to

$$u(z; \nu + \varepsilon) = T_\varepsilon u(z; \nu, \sigma) = \begin{cases} -\frac{z_0(4\nu + 2\varepsilon)}{-2\nu^2 + \frac{1}{2} + z_0^2} + \mathcal{O}((z - z_0)), & \text{if } c = \varepsilon, \\ \varepsilon(z - z_0) + \frac{2(\nu + \varepsilon) + \varepsilon}{2z_0}(z - z_0)^2 + \mathcal{O}((z - z_0)^3) & \text{if } c = -\varepsilon. \end{cases} \quad (79)$$

Thus,  $T_\varepsilon$  transforms poles (or zeros) of  $u(z; \nu, \sigma)$  with residue  $-\varepsilon$  (or  $u' = -\varepsilon$ ) to poles (or zeros) of  $u(z; \nu + 1, \sigma)$  with residue  $+\varepsilon$  (or  $u' = +\varepsilon$ ). This can be confirmed by comparing solutions in Figure 14 (and also in Figure 4) whose  $\nu$ -values differ by an integer. The fact that  $T_\varepsilon$  does not map poles (or zeros) of  $u(z; \nu, \sigma)$  with residue  $\varepsilon$  (or  $u' = \varepsilon$ ) to poles (or zeros) of  $u(z; \nu + 1, \sigma)$  is most easily seen in Figure 4. In the top row of that figure, the poles and zeros that are closest to the imaginary axis, a row of red poles (residue +1) and purple zeros ( $u' = +1$ ), are not mapped to poles and zeros at the corresponding points of the solutions in the second row whose  $\nu$ -values differ by +1.

According to (73), all the pole-free sectors in the first two columns of Figure 14 are scaled and rotated versions of the pole-free sector within  $-\pi/2 < \arg z < \pi/2$  on the 0th sheet. Similarly, according to (75), the pole-free sector within  $-13\pi/2 < \arg z < 14\pi/2$  in the third

to fifth columns is rotationally symmetric, up to a scaling factor, to the pole-free sector on the 0th sheet. However, according to (74), the pole-free sector within  $3\pi < \arg z < 4\pi$  in the third to fifth columns is not a scaled and rotated version of the pole-free sector on the 0th sheet. This asymmetry can be confirmed by comparing the solutions on the centers of these two pole-free sectors: the lines  $\arg z = 0$  and  $\arg z = \frac{7\pi}{2}$ ; the latter line is indicated by red dotted lines in Figure 14. There is one zero, for the  $\nu = -1$  solution, and two zeros, for the  $\nu = -2$  solution, on  $\arg z = \frac{7\pi}{2}$  whereas  $\arg z = 0$  is devoid of zeros for these solutions. Generally, our numerical solutions indicate that on pole-free sectors with  $u \sim \pm i$ ,  $z \rightarrow \infty$ , see Table 2, there are  $|\nu|$  poles or  $|\nu|$  zeros close to  $z = 0$  in the center of the pole-free sector.

Thus far, we have not considered the application of the Bäcklund transformations  $T_0(c_1, e^{-i\theta})$  and  $T_\varepsilon$  to the MTW solutions for the case  $\sigma = \sigma_c$ , see (13) and (14), since then the small- $z$  expansion (8), on which our analysis relies, is not valid. We have found numerically that even if  $\sigma_c$  coincides with one of the values in Table 2, then the MTW solution still has  $n_2$  distinct branches and its pole-free sectors are still described by Table 2. This observation is consistent with the observation made in section 4.2. Namely, if  $0 < \sigma_c = \frac{n_1}{n_2} < 1$ , then the positions of the poles and zeros in the limit  $\sigma \rightarrow \sigma_c$ , given in (32), (33) and (34), repeat every  $n_2$  sheets, in accordance with what one expects if  $z = 0$  is a branch point of order  $n_2$ .

We mention one final empirical observation for the MTW solutions on multiple sheets for the case  $0 < \sigma < 1$ . We found that if  $\nu = 0$ , then the real and imaginary axes on all the sheets are free of poles and zeros. If  $\nu \in \mathbb{Z} \setminus \{0\}$ , then there are no poles or zeros on the real axes but there is no restriction on the number of poles or zeros on the imaginary axes. If  $\nu \in \mathbb{R} \setminus \mathbb{Z}$ , then we found that infinitely many poles or zeros can occur on the real and imaginary axes of sheets other than the 0th sheet.

## 6.4 $\sigma = 1 + 2i\mu$ , $\mu \geq 0$

The pole dynamics on sheet  $s > 0$  for the case  $\sigma = 1 + 2i\mu$ ,  $\mu \geq 0$ , when the small- $z$  behavior on  $\arg z = 0$  is given by (17)–(22), is qualitatively the same for all MTW solutions with  $\nu \in \mathbb{R}$ . After all the transitions through the  $\sigma$  values in Table 2, the poles are aligned along spirals in the  $z$ -plane, see Figure 15. As  $\mu$  increases, the spiral arms move closer to each other, the pole density increases rapidly as the sheet index increases and no pole-free sectors are present on sheets other than the 0th sheet. This suggests that the solution is logarithmically branched if  $|\sigma| \geq 1$  since every sheet appears to be distinct.

## 7 Conclusion

The MTW solutions were first studied asymptotically on the positive real axis in [25]. Their asymptotics in the right half-plane follow from the recent results in [22]. Our enhanced PFS method completes this progression since it has enabled the study of the MTW tronquée solutions of  $P_{\text{III}}$  on their Riemann surfaces. A new result of this study is the asymptotics of the MTW solutions on multiple Riemann sheets, which follow from Theorems 1 and 2 and which are given in Proposition 1 and Table 2.

We also found solution features that were not seen in the computational studies of the single-valued Painlevé transcendents in [11–13, 32–34]. This is to be expected from the added complexity that the fixed singularity of the  $P_{\text{III}}$  equation at  $z = 0$  can give rise to: a branch point and thus a possible infinitude of distinct solution branches and a potential limit point of poles or zeros. One basic difference is that poles and zeros of multivalued  $P_{\text{III}}$  solutions can enter or leave a bounded region through a branch point and a branch cut as the parameters are varied (see Figures 1 and 2 for examples). For the class of  $P_{\text{III}}$  solutions that we explored,

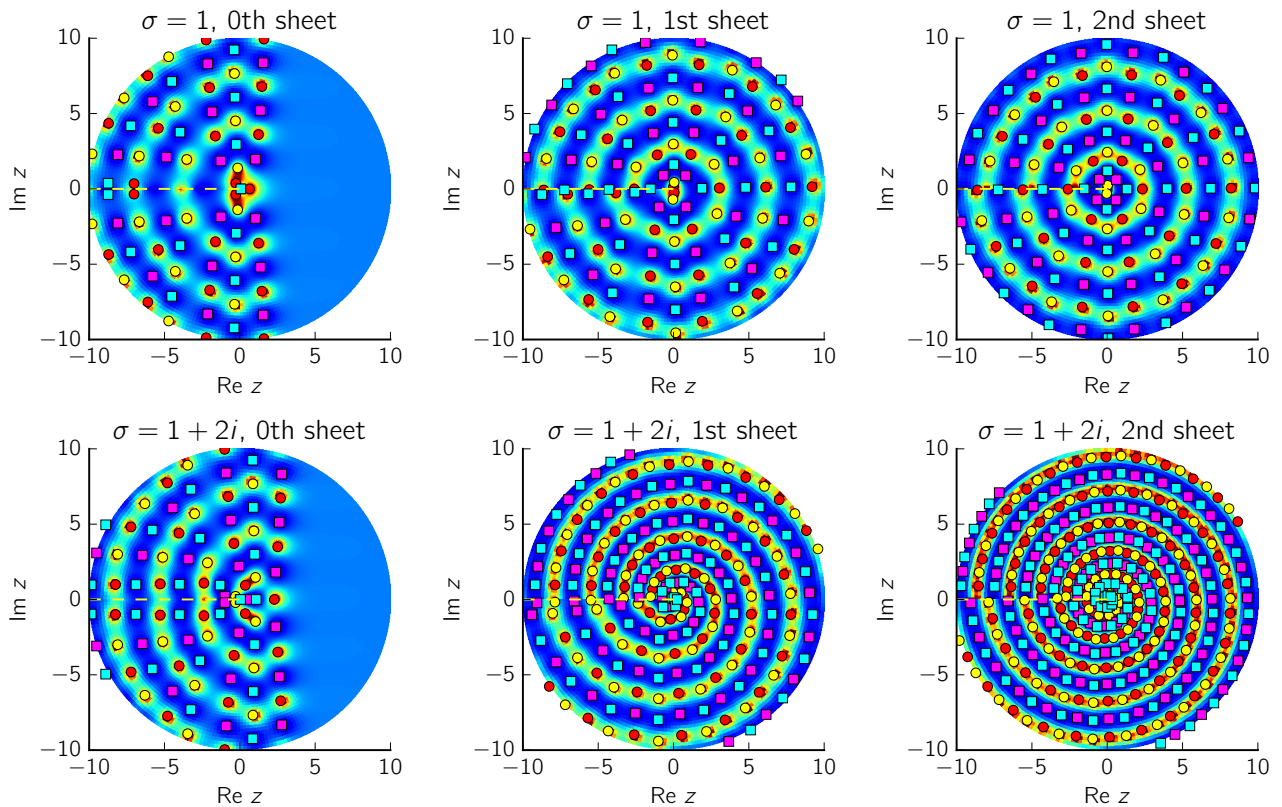


Figure 15: The typical pole dynamics of an MTW solution for the case  $|\sigma| \geq 1$  on multiple sheets (for this solution  $\nu = -5/4$ ).

the branch point can be a source of infinitely many poles or zeros on the positive real axis. By contrast, in single-valued solutions, poles and zeros can only enter or exit a bounded region through the boundary of the domain. Transitions through tronquée solutions for large- $z$  with its associated change in pole field alignment, see Figure 12, are also features of the meromorphic Painlevé transcendents. However, for  $P_{\text{III}}$  solutions tronquée transitions also occur for small  $z$  (see Figure 8 and recall that  $z = e^{\zeta/2}$ ) during which poles and zeros coalesce at  $z = 0$ , which is another solution feature that was not observed in the numerical studies of the meromorphic Painlevé transcendents.

We found symmetries or asymmetries between different sheets of the same solution (Figure 14), the same sheets of different solutions (Figure 14) and different sheets of different solutions (Figure 13). These global properties of the solutions could be explained using small- $z$  asymptotics and Bäcklund transformations. To our knowledge the pole-free sectors in Table 2 have not been noted in the literature before (except for the pole-free sector on the 0th sheet which follows from the results in [22]). We also quantified changes in these pole-free regions as functions of the parameters in sections 3.1.1, 3.2 and 4.1.

We hope that our analytical and computational results will clear up a misconception in the literature (e.g., in [23, 26]) regarding the order of algebraic branch points that are admitted by  $P_{\text{III}}$  at  $z = 0$ : algebraic branch points of any order, not just order three, are possible (see Corollary 1 and an example in Figure 13).

Many types of  $P_{\text{III}}$  solutions remain to be explored (not to mention the unexplored solution spaces of  $P_{\text{V}}$  and  $P_{\text{VI}}$ ). These include tronquée solutions for the cases  $\gamma\delta \neq 0$ ,  $\alpha \neq -\beta$  and  $\gamma = 0$ ,  $\alpha\delta \neq 0$  (see Theorem 2 in [22]); single-valued solutions [15, pp.151–154]; triply branched solutions [5, 23], special function solutions [26] and generic solutions that fall into none of these categories.

## Acknowledgements

The research of J.A.C. Weideman is supported in part by the National Research Foundation of South Africa (Grant Number 103321). We are also indebted to the anonymous referees for their helpful remarks and suggestions.

## References

- [1] M.J. Ablowitz and H. Segur. Asymptotic solutions of the Korteweg–de Vries equation. *Stud. Appl. Math.*, 57(1):13–44, 1977.
- [2] F.V. Andreev and A.V. Kitaev. Exponentially small corrections to divergent asymptotic expansions of solutions of the fifth Painlevé equation. *Math. Res. Lett.*, 4(5):741–759, 1997.
- [3] E. Barouch, B.M. McCoy, and T.T. Wu. Zero-field susceptibility of the two-dimensional Ising model near  $T_c$ . *Phys. Rev. Lett.*, 31(23):1409–1411, 1973.
- [4] P. Boutroux. Recherches sur les transcendentes de M. Painlevé et l’étude asymptotique des équations différentielles du second ordre. *Ann. École Norm.*, 30:255–375, 1913.
- [5] P.A. Clarkson. The third Painlevé equation and associated special polynomials. *J. Phys. A: Math. Gen.*, 36(36):9507–9532, 2003.
- [6] P.A. Clarkson. Painlevé equations–nonlinear special functions. In F. Marcellán and W. van Assche, editors, *Orthogonal Polynomials and Special Functions: Computation and Application*, volume 1883 of *Lecture Notes in Math.*, pages 331–411. Springer, Berlin, 2006.
- [7] D. Dai and L. Zhang. On tronquée solutions of the first Painlevé hierarchy. *J. Math. Anal. Appl.*, 368(2):393–399, 2010.
- [8] NIST Digital Library of Mathematical Functions. <http://dlmf.nist.gov/>, Release 1.0.10 of 2015-08-07. Online companion to [28].
- [9] M. Fasoldini, B. Fornberg, and J.A.C. Weideman. Methods for the computation of the multivalued Painlevé transcendents on their Riemann surfaces. *J. Comput. Phys.*, 344:36–50, 2017.
- [10] A.S. Fokas, A.R. Its, A.A. Kapaev, and V.Y. Novokshënov. *Painlevé Transcendents: The Riemann-Hilbert Approach*, volume 128 of *Mathematical Surveys and Monographs*. American Mathematical Society, Providence, RI, 2006.
- [11] B. Fornberg and J.A.C. Weideman. A numerical methodology for the Painlevé equations. *J. Comput. Phys.*, 230:5957–5973, 2011.
- [12] B. Fornberg and J.A.C. Weideman. A computational exploration of the second Painlevé equation. *Found. Comput. Math.*, 14(5):985–1016, 2014.
- [13] B. Fornberg and J.A.C. Weideman. A computational overview of the solution space of the imaginary Painlevé II equation. *Physica D*, 309:108–118, 2015.
- [14] B. Gambier. Sur les équations différentielles du second ordre et du premier degré don’t l’intégrale générale est à points critiques fixés. *Acta Math.*, 33(1):1–55, 1910.

- [15] V.I. Gromak, I. Laine, and S. Shimomura. *Painlevé Differential Equations in the Complex Plane*. Walter de Gruyter, Berlin, 2002.
- [16] A. Hinkkanen and I. Laine. Solutions of a modified third Painlevé equation are meromorphic. *J. Anal. Math.*, 85:323–337, 2001.
- [17] N. Joshi. Tritronquée solutions of perturbed first Painlevé equations. *Theoret. and Math. Phys.*, 137(2):1515–1519, 2003.
- [18] N. Joshi and A.V. Kitaev. On Boutroux’s tritronquée solutions of the first Painlevé equation. *Stud. Appl. Math.*, 107(3):253–291, 2001.
- [19] N. Joshi and M. Mazzocco. Existence and uniqueness of tri-tronquée solutions of the second Painlevé hierarchy. *Nonlinearity*, 16(2):427, 2002.
- [20] N. Joshi and T. Morrison. Existence and uniqueness of tronquée solutions of the fourth-order Jimbo–Miwa second Painlevé equation. *Proc. Amer. Math. Soc.*, 137(6):2005–2014, 2009.
- [21] D. Levi and P. Winternitz, editors. *Painlevé Transcendents: Their Asymptotics and Physical Applications*, volume 278. Springer Science & Business Media, 2013.
- [22] Y. Lin, D. Dai, and P. Tibboel. Existence and uniqueness of tronquée solutions of the third and fourth Painlevé equations. *Nonlinearity*, 27(2):171–186, 2014.
- [23] N.A. Lukashovich. On the theory of the third Painlevé equation. *Differential Equations*, 3:994–999, 1967.
- [24] B. M. McCoy, J. H. H. Perk, and R. E. Shrock. Time-dependent correlation functions of the transverse Ising chain at the critical magnetic field. *Nuclear Phys. B*, 220(1):35–47, 1983.
- [25] B.M. McCoy, C.A. Tracy, and T.T. Wu. Painlevé functions of the third kind. *J. Math. Phys.*, 18(5):1058–1092, 1977.
- [26] A.E. Milne, P.A. Clarkson, and A.P. Bassom. Bäcklund transformations and solution hierarchies for the third Painlevé equation. *Stud. Appl. Math.*, 98:139–194, 1997.
- [27] J.M. Myers. Wave scattering and the geometry of a strip. *J. Math. Phys.*, 6(11):1839–1846, 1965.
- [28] F.W.J. Olver, D.W. Lozier, R.F. Boisvert, and C.W. Clark, editors. *NIST Handbook of Mathematical Functions*. Cambridge University Press, New York, NY, 2010. Print companion to [8].
- [29] P. Painlevé. Mémoire sur les équations différentielles dont l’intégrale générale est uniforme. *Bull. Soc. Math.*, 28:201–261, 1900.
- [30] P. Painlevé. Sur les équations différentielles du second ordre et d’ordre supérieur dont l’intégrale générale est uniforme. *Acta Math.*, 25(1):1–85, 1902.
- [31] S. Persides and B.C. Xanthopoulos. Some new stationary axisymmetric asymptotically flat space-times obtained from Painlevé transcendents. *J. Math. Phys.*, 29(3):674–680, 1988.

- [32] J.A. Reeger. *A Computational Study of the Fourth Painlevé Equation and a Discussion of Adams Predictor-Corrector Methods*. PhD thesis, University of Colorado, 2013.
- [33] J.A. Reeger and B. Fornberg. Painlevé IV with both parameters zero: A numerical study. *Stud. Appl. Math.*, 130(2):108–133, 2013.
- [34] J.A. Reeger and B. Fornberg. Painlevé IV: A numerical study of the fundamental domain and beyond. *Physica D*, 280–281:1–13, 2014.
- [35] S. Shimomura. Truncated solutions of the fifth Painlevé equation. *Funkcialaj Ekvacioj*, 54(3):451–471, 2011.
- [36] E. Wegert. *Visual Complex Functions: An Introduction with Phase Portraits*. Birkhäuser/Springer Basel AG, Basel, 2012.
- [37] T.T. Wu, B.M. McCoy, C.A. Tracy, and E. Barouch. Spin-spin correlation functions for the two-dimensional Ising model: Exact theory in the scaling region. *Phys. Rev. B*, 13:316–374, 1976.
- [38] A.B. Zamolodchikov. Painlevé III and 2D polymers. *Nuclear Phys. B*, 432(3):427–456, 1994.

## Appendix

Lemma 2 below is used in the proofs of Theorem 1 in section 6.2 and Theorem 3 in this appendix. Although Theorem 3 below is referred to in section 5.1, we recommend that its proof be read in conjunction with the proof of Theorem 1 in the later section 6.2 since similar ideas are used. The final result below, Lemma 3, is used in section 5.2 and its proof is independent of any results in this appendix.

**Lemma 2.** *Let  $\nu \in \mathbb{R}$  and  $0 < \sigma < 1$  or  $\sigma = 1 + 2i\mu$ ,  $\mu > 0$ , then  $B(\sigma, -\nu) = B(\sigma, \nu)$  if and only if  $\nu \in \mathbb{Z}$  and  $B(\sigma, -\nu) = -B(\sigma, \nu)$  if and only if  $\nu = n + \frac{1}{2}$ ,  $n \in \mathbb{Z}$ .*

*Proof.* It follows from the definition of  $B(\sigma, \nu)$  in (12) and the identity  $\Gamma(z)\Gamma(1-z) = \pi/\sin(\pi z)$  [8] that

$$B(\sigma, \nu) + B(\sigma, -\nu) = 2B(\sigma, \nu)R(\sigma, \nu), \quad R(\sigma, \nu) := \frac{\cos(\pi\sigma/2)\cos(\pi\nu)}{\cos[\pi(\sigma/2 - \nu)]}.$$

For  $0 < \sigma < 1$  or  $\sigma = 1 + 2i\mu$ ,  $\mu > 0$ , the zeros and singularities of  $B(\sigma, \nu)$  occur only at  $\sigma_c$ , defined in (13) and (14), see (12) and (21). Hence, we exclude  $\sigma = \sigma_c$  in which case  $0 < |B(\sigma, \nu)| < \infty$ . Also note that if  $\sigma \neq \sigma_c$ , then  $\cos[\pi(\sigma/2 - \nu)] \neq 0$  and thus  $|R(\sigma, \nu)| < \infty$ . Hence, for  $\nu \in \mathbb{R}$  and  $0 < \sigma < 1$  or  $\sigma = 1 + 2i\mu$ ,  $\mu > 0$  with  $\sigma \neq \sigma_c$  we have

$$B(\sigma, -\nu) = B(\sigma, \nu) \Leftrightarrow R(\sigma, \nu) = 1 \Leftrightarrow \cos(\pi\sigma/2)\cos(\pi\nu) = \cos[\pi(\sigma/2 - \nu)] \Leftrightarrow \nu \in \mathbb{Z},$$

and

$$B(\sigma, -\nu) = -B(\sigma, \nu) \Leftrightarrow R(\sigma, \nu) = 0 \Leftrightarrow \cos(\pi\nu) = 0 \Leftrightarrow \nu = n + \frac{1}{2}, \quad n \in \mathbb{Z}.$$

□

**Theorem 3.** *The left-end MTW solution,  $u(z; -\nu, \sigma)$ , where  $\nu = \frac{1}{2} + n$ ,  $n \geq 0$ , and the MTW solution  $u(z; \nu, \sigma)$  are related according to*

$$u(z; -\nu, \sigma) = T_0(-1, 1)u(z; \nu, \sigma) = -u(z; \nu, \sigma). \quad (80)$$

*Proof.* According to Lemma 1, the result follows if (51) holds. For the transformation  $T_0(-1, 1)$ ,  $\tilde{\nu} = -\nu$ ,  $c_1 = -1$  and  $c_2 = e^{-i\theta} = 1$  and thus (51) becomes

$$B(\sigma, -\nu) = -B(\sigma, \nu). \quad (81)$$

It follows from Lemma 2 that this equations is satisfied for  $0 < \sigma < 1$  or  $\sigma = 1 + 2i\mu$ ,  $\mu > 0$  only if  $\nu = \frac{1}{2} + n$ ,  $n \in \mathbb{Z}$ .

For  $\sigma = 1$ , the condition (81) is not valid since  $B(\sigma, \nu)$  is undefined according to (12). To prove (80) for  $\sigma = 1$ , it is sufficient to show (by the same argument used in the proof of Lemma 1) that the leading order terms of the  $\sigma = 1$  small- $x$  expansions on the left and right-hand sides of (80) match. We show this as follows. If  $\sigma = 1$ , then the small- $x$  behaviour of MTW solutions is given by (17) and as  $x \rightarrow 0^+$

$$u(x/2; \nu, \sigma) + u(x/2; -\nu, \sigma) \sim \frac{x}{2} [C(\nu) + C(-\nu)] \left\{ -\ln x + \frac{1}{4\nu} [C(\nu) - C(-\nu)] \right\}, \quad \sigma = 1. \quad (82)$$

It follows from the definition of  $C(\nu)$  in (18) and the identities [8]

$$\psi(z+1) = \psi(z) + \frac{1}{z}$$

and

$$\psi(z) - \psi(1-z) = -\frac{\pi}{\tan(\pi z)}$$

that

$$C(\nu) + C(-\nu) = \frac{2\pi\nu}{\tan \pi\nu}, \quad (83)$$

which is zero only if  $\nu = n + \frac{1}{2}$ ,  $n \in \mathbb{Z}$ . Comparing (83) and (82), we conclude that the leading order terms of  $u(z; -\nu, \sigma)$  and  $-u(z; \nu, \sigma)$  match as  $x \rightarrow 0^+$  only if  $\nu = n + \frac{1}{2}$ ,  $n \in \mathbb{Z}$ .  $\square$

**Lemma 3.** Let  $u(z; -1, 1, 1, -1)$  be the solution defined in (40) and let  $p_n(z) = \sum_{j=0}^n c_j z^{n-j}$ , where the coefficients  $c_j$  are defined by (6) with  $\nu = -\frac{1}{2} - n$ , i.e.,

$$c_{j+1} = -\frac{(n-j)^2}{4(j+1)} c_j, \quad 0 \leq j \leq n-1, \quad c_0 = 1. \quad (84)$$

Then

$$u(z; -1 - 2n, 1 + 2n, 1, -1) = T_{-1}^n u(z; -1, 1, 1, -1) = 1 - CP_n(z)e^{-2z} + \mathcal{O}(e^{-4z}), \quad (85)$$

for  $z \rightarrow \infty$ ,  $-\frac{\pi}{2} < \arg z < \frac{\pi}{2}$ , where  $P_n(z) = \frac{(-4)^n}{n!} p_n(z)$ .

*Proof.* We prove the result by induction. Since  $p_0(z) = c_0 = 1$ , it follows from (39) and (40) that  $P_0(z) = p_0(z)$  if we set  $k = C$  and thus the result is valid for  $n = 0$ . Let  $P_n(z) = \sum_{j=0}^n c_j^{(n)} z^{n-j}$  and suppose that (85) holds for some  $n \geq 1$  with  $P_n(z) = \frac{(-4)^n}{n!} p_n(z)$  if we set  $k = C$ . Then, substituting (85) into the Bäcklund transformation (38) with  $\varepsilon = -1$ , we find that

$$\begin{aligned} u(z; -1 - 2(n+1), 1 + 2(n+1), 1, -1) &= T_{-1} u(z; -1 - 2n, 1 + 2n, 1, -1) \\ &= 1 - CP_{n+1}(z)e^{-2z} + \mathcal{O}(e^{-4z}), \quad z \rightarrow \infty, \quad -\frac{\pi}{2} < \arg z < \frac{\pi}{2}, \end{aligned}$$

where

$$P_{n+1}(z) = P_n(z) - \frac{z}{n+1} [4P_n(z) - P_n'(z)]. \quad (86)$$

The recurrence (86) implies that

$$c_{k+1}^{(n+1)} = c_k^{(n)} - \frac{4}{n+1}c_{k+1}^{(n)} + \frac{n-k}{n+1}c_k^{(n)}, \quad 0 \leq k \leq n-1, \quad c_0^{(n+1)} = -\frac{4}{n+1}c_0^{(n)}, \quad c_{n+1}^{(n+1)} = c_n^{(n)}. \quad (87)$$

Since we assume that  $P_n(z) = \frac{(-4)^n}{n!}p_n(z)$ , the formula (84) also holds for the coefficients of  $P_n(z)$ , except that  $c_0^{(n)} = \frac{(-4)^n}{n!}$ . Using this and (87) it is straightforward to show that

$$c_{j+1}^{(n+1)} = -\frac{(n+1-j)^2}{4(j+1)}c_j^{(n+1)}, \quad 0 \leq j \leq n, \quad c_0^{(n+1)} = \frac{(-4)^{n+1}}{(n+1)!}. \quad (88)$$

Comparing (88) and (84) with  $n+1$  we deduce that  $P_{n+1}(z) = \frac{(-4)^{n+1}}{(n+1)!}p_{n+1}(z)$ , which concludes the proof.  $\square$